CHAPTER 5
AZITHROMYCIN GLASS

5.1 Introduction

Amorphous solids have become an important consideration in the pharmaceutical industry. The necessity to overcome unwanted effects (i.e. low water solubility, slow dissolution rates or poor bioavailability), resulting from the physical and chemical properties of crystalline forms, has become a significant driving force in discovering and developing amorphous forms. Numerous studies of amorphous forms of APIs have reported improved pharmaceutical properties of that given API (Threlfall, 1995:2452).

The physical and chemical properties of the amorphous solid(s) of any drug differ substantially from those of its crystalline counterpart(s). The structural and chemical stabilities of amorphous solids usually pose limitations, since amorphous solids tend to be thermodynamically unstable in comparison with their crystalline equivalents. The rapid cooling from the melt method is considered suitable for preparing more stable, amorphous solids (glasses). Despite the fact that a glass presents structurally as more liquid-like, its behaviour relates to that of a solid. Improved solubility is often the essential consequence of an amorphous solid, due to high potential free energy. This is especially significant when a compound is poorly soluble in water. Enhanced solubility holds the advantage of improving the bioavailability for these compounds (Cui, 2007:11; Vippagunta *et al*., 2001:3; Wu *et al*., 2010:4).

Careful consideration is essential, since the improved solubility of an amorphous solid, due to its higher free energy, is usually overshadowed by chemical instability and time dependent transformation into the thermodynamically more stable, crystalline form. It is therefore important to determine the physical and chemical stabilities of the amorphous state of a given API (Cui, 2007:11; Vippagunta *et al*., 2001:3; Wu *et al*., 2010:4).

A new amorphous glassy form of azithromycin (AZM-G) was prepared during this study. This chapter covers the characterisation of AZM-G, the determination of its solubility in various aqueous media, the stability of AZM-G at high relative humidity and temperature, exposure to increased water fractions and direct exposure to water for a period of 20 days. The extent and rate of degradation of AZM-G in 0.1 M hydrochloric acid (HCl) were also established.

5.2 Method for the preparation of azithromycin glass (AZM-G)

AZM-DH powder was evenly sprinkled on an aluminium foil pan in a thin layer, where after it was placed in a conventional oven (dry heat) that had been pre-heated at 130˚C. This set temperature was higher than the determined melting point (119.04˚C) of AZM-DH (Section 5.3.3). The AZM-DH powder was allowed sufficient time to dehydrate and to melt. The melt was then removed from the oven and allowed to cool to room temperature. During cooling the melt transformed into a solid (afterwards characterised as a supercooled solid) that presented as a glass. This complete process is described in the International Patent application (PCT/IB2010/055842) (Annexure B: only first page of PCT included due to length of application). Due to the fact that AZM-DH was subjected to a relatively high temperature during the preparation of AZM-G, an HPLC assay was used to determine the integrity and purity of the prepared AZM-G. The results indicated that temperature had no degrading effect on AZM-G and was the purity being established as 97.5 % of azithromycin.

5.3 Solid state characterisation of azithromycin glass (AZM-G)

5.3.1 Fourier transform infrared spectroscopy (FTIR)

The FTIR spectrum of AZM-DH is presented in Figure 5.1 and displays characteristic sharp peaks at 3567 cm^{-1} and 3496 cm^{-1} and another sharp peak at 1720 cm^{-1}. A relatively broad peak is found at 3251 cm^{-1}, whilst the peak at 2971 cm^{-1} is also of interest, when compared to Figure 5.2 (see Table 5.1 also). The two sharp peaks at 3567 cm^{-1} and 3496 cm^{-1} were representative of the two water molecules of AZM-DH, as they occurred within the OH-stretching region (Brittain, 1999:260; Gandhi *et al*., 2002:182; West, 1999:180). In the event of a change in hydration/dehydration of AZM, the difference in the hydrated state can be determined by studying the spectral area between wavenumbers 3600 - 3000 cm^{-1}, i.e. the OH-stretching region (Gandhi *et al*., 2002:182).

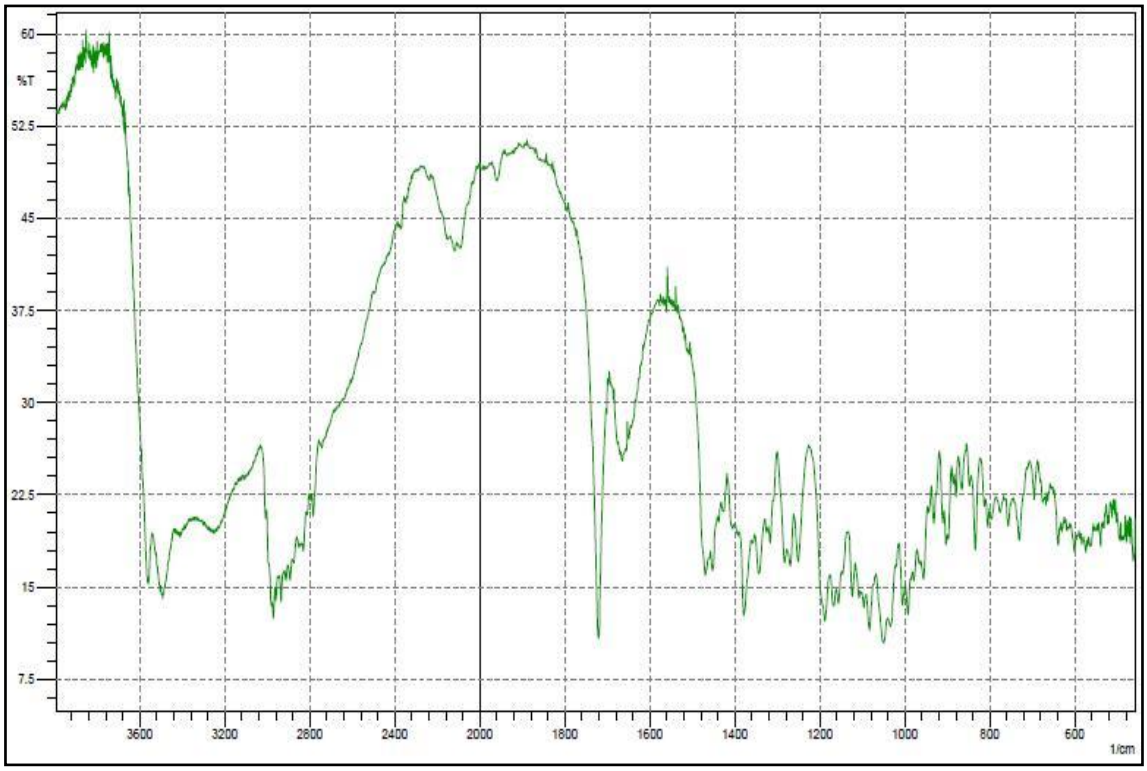

Figure 5.1 FTIR spectrum of AZM-DH.

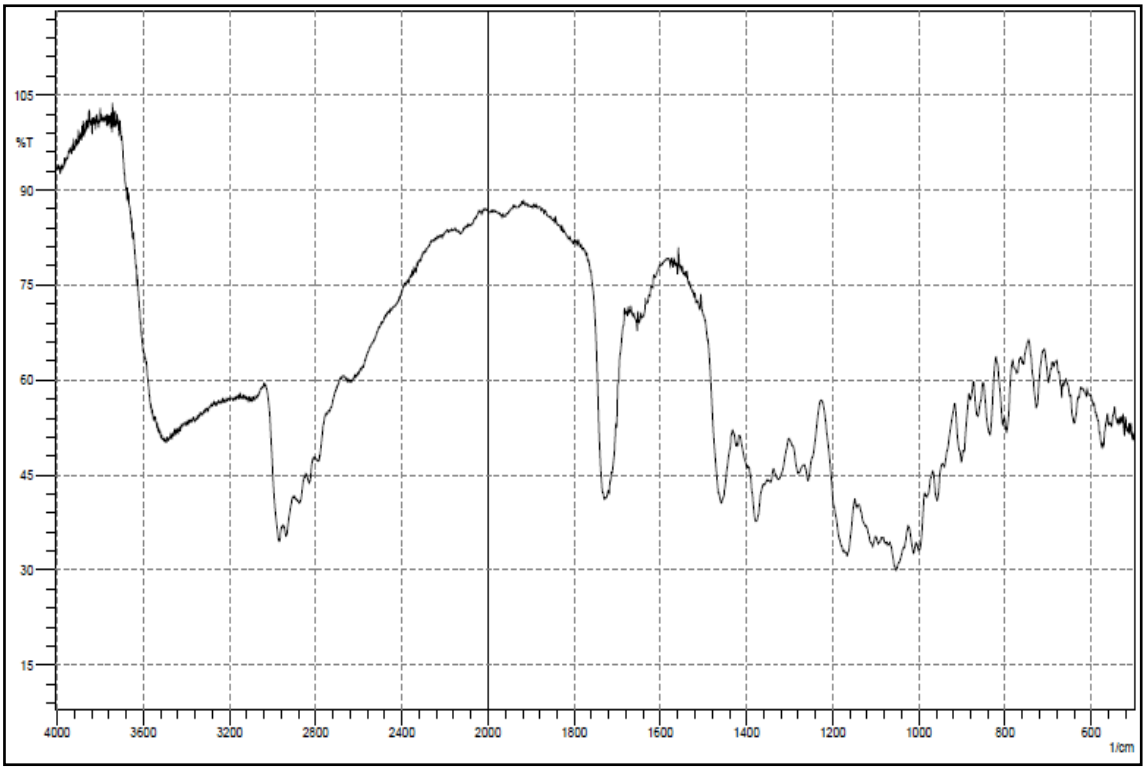

Figure 5.2 FTIR spectrum of AZM-G.

The most distinguishing differences between the FTIR patterns of AZM-DH (Figure 5.1) and AZM-G (Figure 5.2) were between wavenumbers 3580 - 1727 cm^{-1} (Table 5.1). The

FTIR pattern of AZM-DH (Figure 5.1) displayed five separate, clearly distinguishable peaks at 3567, 3496, 3251, 2971 and 1720 cm^{-1} (Table 5.1). This contrasted with the amorphous AZM-G that displayed peaks at 3500 (broad peak), 2970, 2938 and 1727 cm^{-1} (broad peak) (Table 5.1). In contrast with Figure 5.1, Figure 5.2 displayed only one broad peak at wavenumber 3500 cm^{-1} and no peak at 3251 cm^{-1}, which were indicative of a lack of hydrated molecules in AZM-G. This data also correlated well with the fact that peak broadening occurs in amorphous forms of a drug and not in its crystalline counterparts (Chieng *et al*., 2011:620; Yu *et al*., 1998:124).

The water content of this amorphous sample was determined by KFT. The results indicated a complete absence of water. The AZM-G spectrum being generated during this study further showed similarities to that of anhydrous AZM reference material, as reported by Khan *et al*. (2002:12). This meant that the FTIR spectrum of AZM-G could be used as reference for identification when determining the hydration state of different forms of AZM. The broadened peaks at 3500 cm^{-1} and 1727 cm^{-1} (Table 5.1) on the AZM-G spectrum also accentuated the amorphous nature of this unique form of AZM (Chieng *et al*., 2011:620; Yu *et al*., 1998:124).

Table 5.1 Peak differences in FTIR patterns to distinguish between AZM-DH and AZM-G

AZM-DH	AZM-G
3567 and 3496 cm^{-1} (sharp peaks)	3500 cm^{-1} (relatively broad peak)
3251 cm^{-1} (relatively broad peak)	No peak
2971 cm^{-1}	2970 and 2938 cm^{-1}
1720 cm^{-1} (sharp peak)	1727 cm^{-1} (relatively broad peak)

5.3.2 X-ray powder diffraction (XRPD)

The XRPD pattern acquired for AZM-DH is presented in Figure 5.3 and illustrates peaks that are characteristic of its crystalline nature. These peaks with variable intensities were detected at various scattering angles (degrees 2θ).

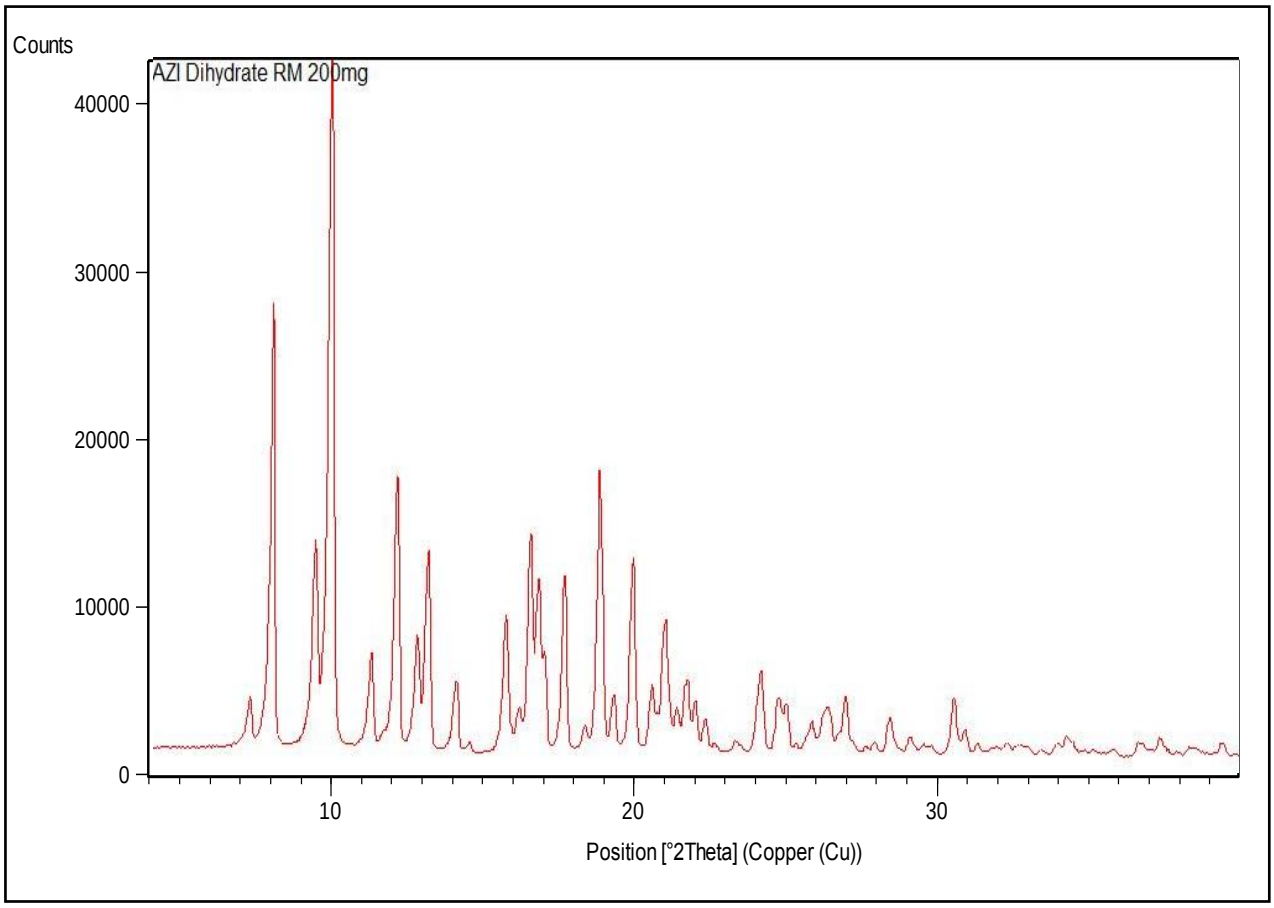

Figure 5.3 XRPD pattern of AZM-DH.

Whilst the XRPD pattern of AZM-G showed no characteristic peaks (Figure 5.4), the diffractogram showed a typical amorphous halo pattern (Byrn *et al*., 1999:249; Chieng *et al*., 2011:620). The absence of peaks on the XRPD pattern meant that there was no long-range order of molecular packing, as in the crystalline form and therefore AZM-G could be regarded as amorphous (Byrn *et al*., 1999:22; Yu, 2001:27).

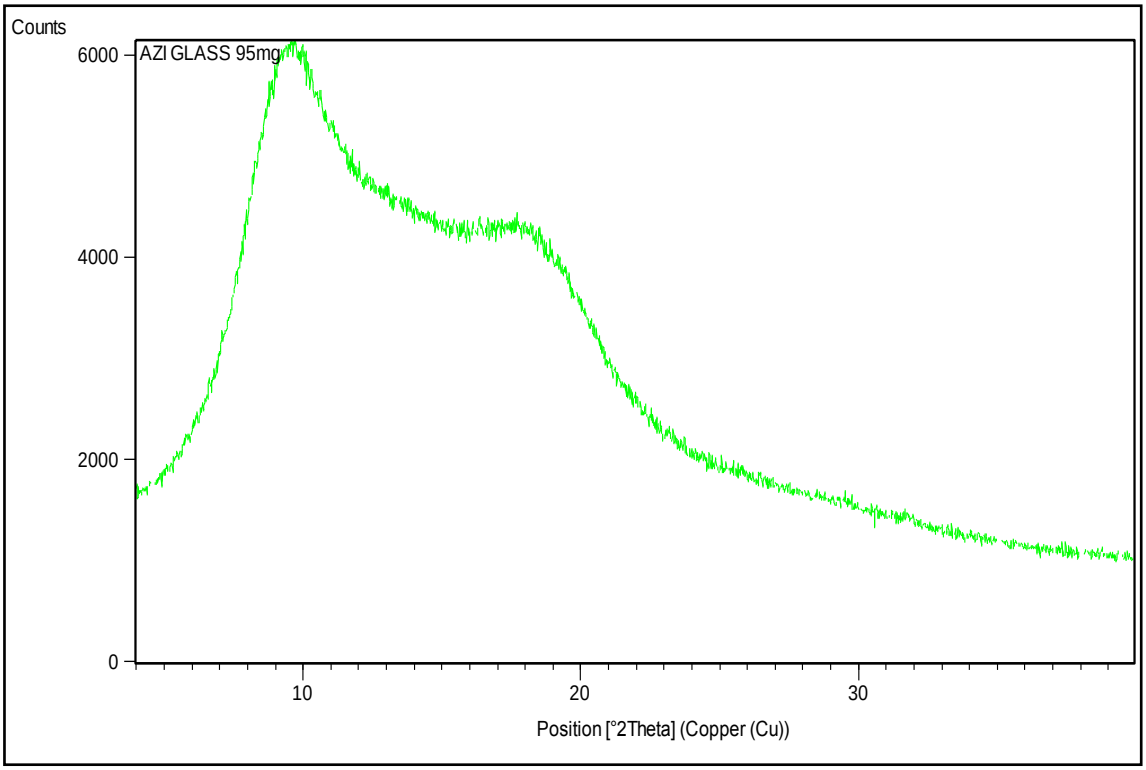

Figure 5.4 XRPD pattern of AZM-G.

5.3.3 Differential scanning calorimetry (DSC)

With regards to Figure 5.5, the DSC thermogram of AZM-DH showed two dehydration peaks (endotherms) of the dihydrate at 76.35˚C and 86.45˚C. The first broad endotherm at 76.35˚C suggested the conversion of the dihydrate into the less stable monohydrate. The conversion from the newly formed monohydrate into the anhydrous form was signified by the second smaller endotherm (86.45˚C). These two endotherms (dehydration) were followed by the subsequent melting event of AZM-DH (Gandhi *et al*., 2002:180), with the melting point of AZM-DH being observed at 119.04˚C (Figure 5.5).

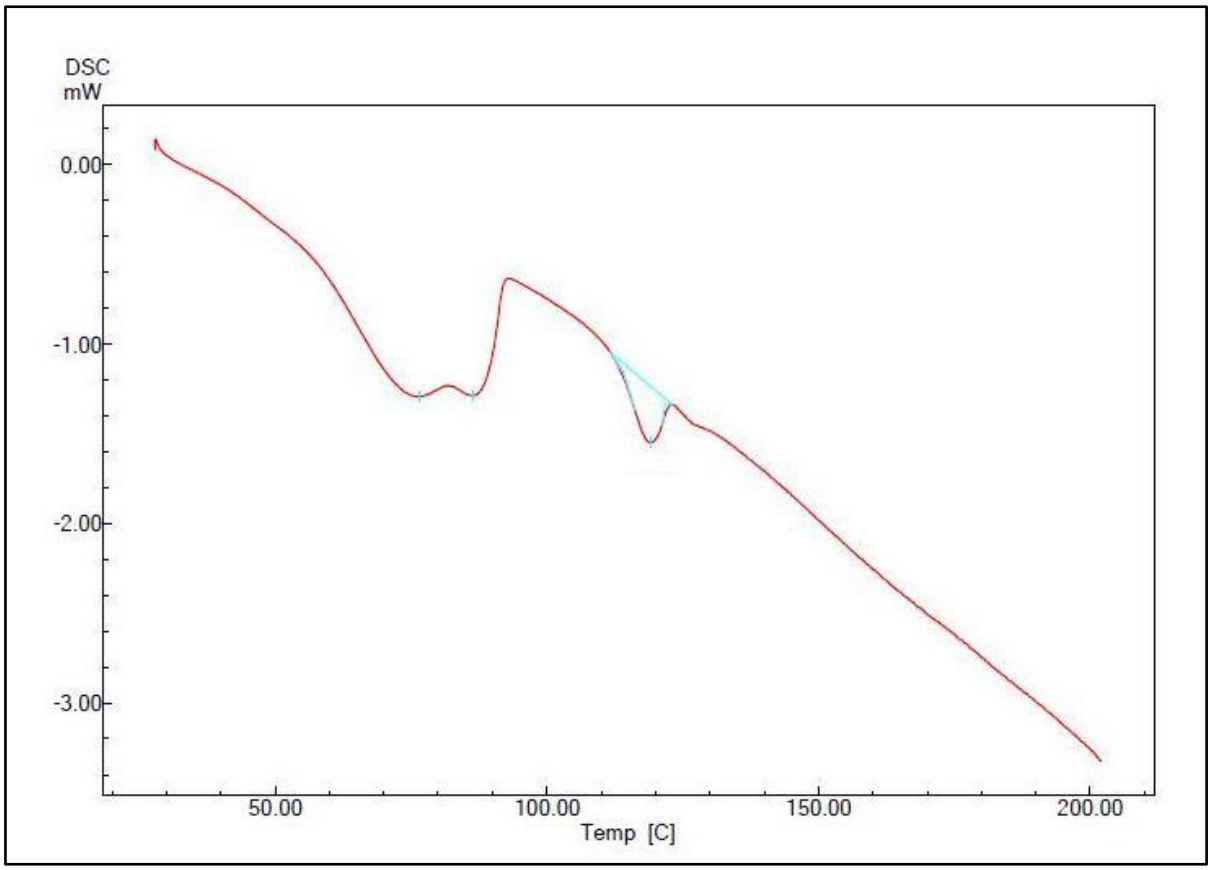

Figure 5.5 DSC trace of AZM-DH showing dehydration at 76.35˚C and 86.45˚C and the subsequent melting endotherm at 119.04˚C.

Figure 5.6 shows the DSC trace of amorphous AZM-G, on which the two dehydration endotherms, visible on the DSC trace of AZM-DH (Figure 5.5), were absent. No crystalline melting peak was observed. The AZM-G trace further displayed a glass transition at 106.65˚C. The glass transition temperature (T_g) of 106.65˚C signified the event where the solid glass form submitted to a transition into the liquid state. From this data it could be concluded that AZM-G was completely amorphous. The transition was due to increased molecular mobility, as a result of the increase in temperature (Yu, 2001:32). According to Craig *et al*. (1999:194), optimum crystal growth is achieved at temperatures between the T_g of the amorphous glass and the melting point (T_m) of the crystalline state. If crystallisation should occur, it would therefore be between 106.65°C and 119.04°C. The absence of a recrystallisation peak on the DSC trace of AZM-G may thus have been indicative of the stability of AZM-G in its amorphous state.

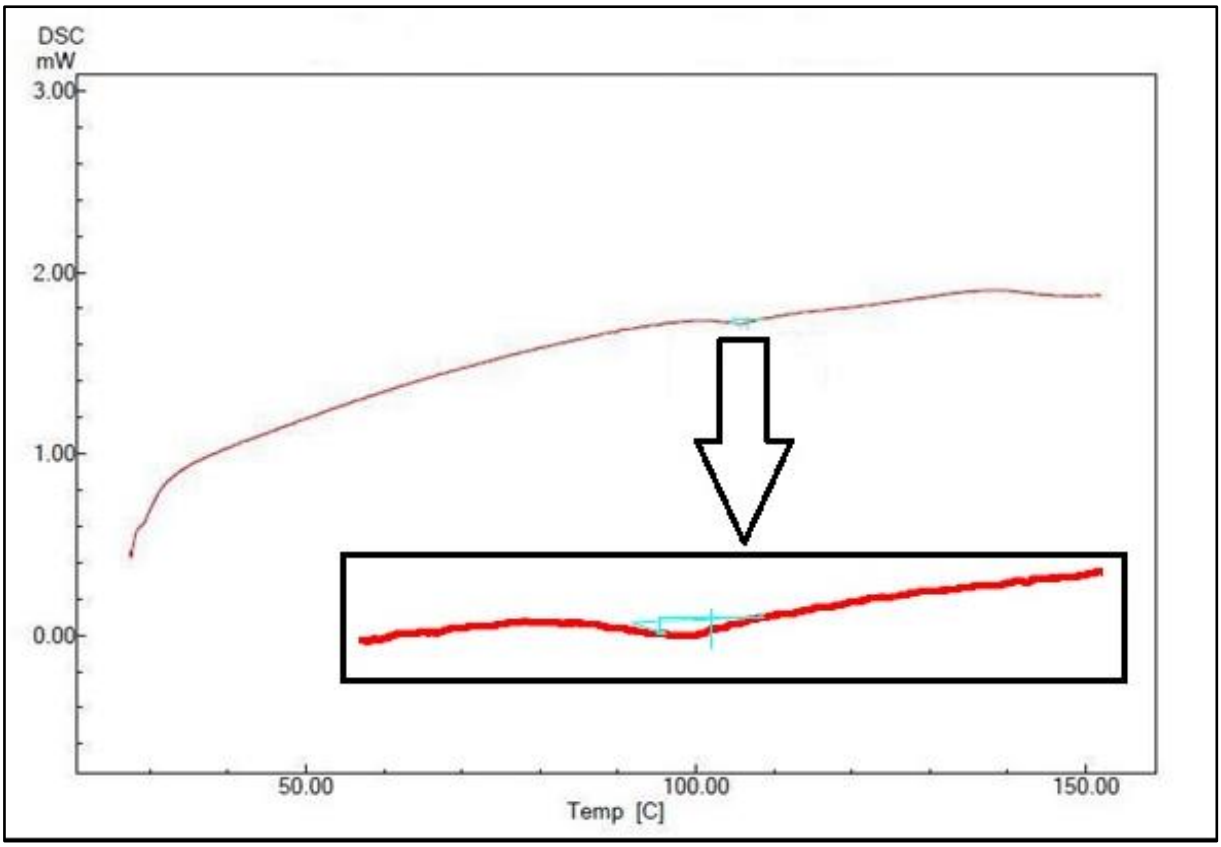

Figure 5.6 DSC trace of AZM-G with T_g (enhanced trace) at 106.65°C.

5.3.4 Thermogravimetric analysis (TGA)

The outcome of TG analysis of AZM-DH is illustrated in Figure 5.7. The 4.40 % loss, expressed as a percentage of the initial sample weight, can be attributed to the loss of two water molecules upon dehydration. This correlated well with the calculated theoretical weight loss of 4.59 %, as stipulated by the USP (2010). As seen in Figure 5.7, the onset of weight loss was at approximately 70˚C, which related to the start of the dehydration event. Compared to the DSC trace, which clearly indicated the dehydration process (two endotherms on Figure 5.5) at 76.35˚C, this TGA result confirmed the DSC findings by (Gandhi *et al*., 2002:179) (Section 5.3.3).

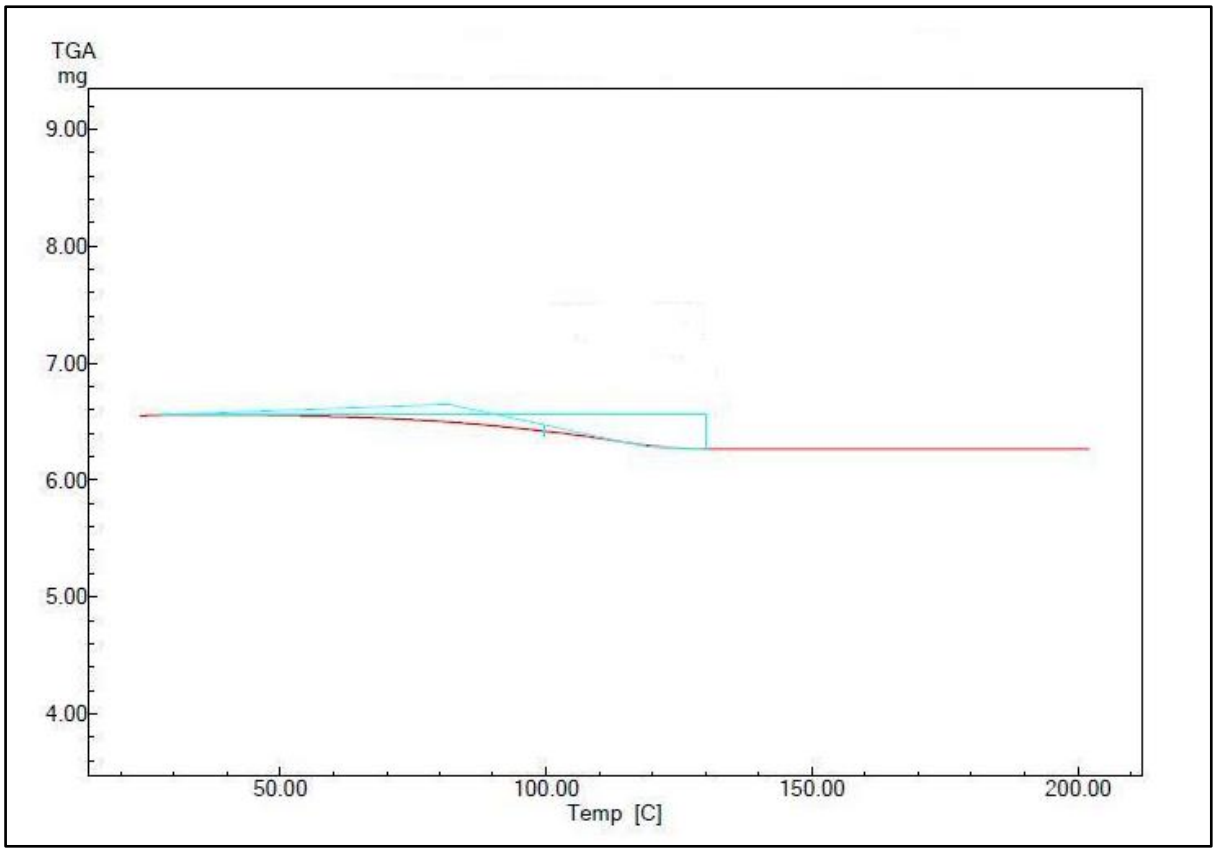

Figure 5.7 TGA thermogram of AZM-DH indicating a weight loss of 4.40 %.

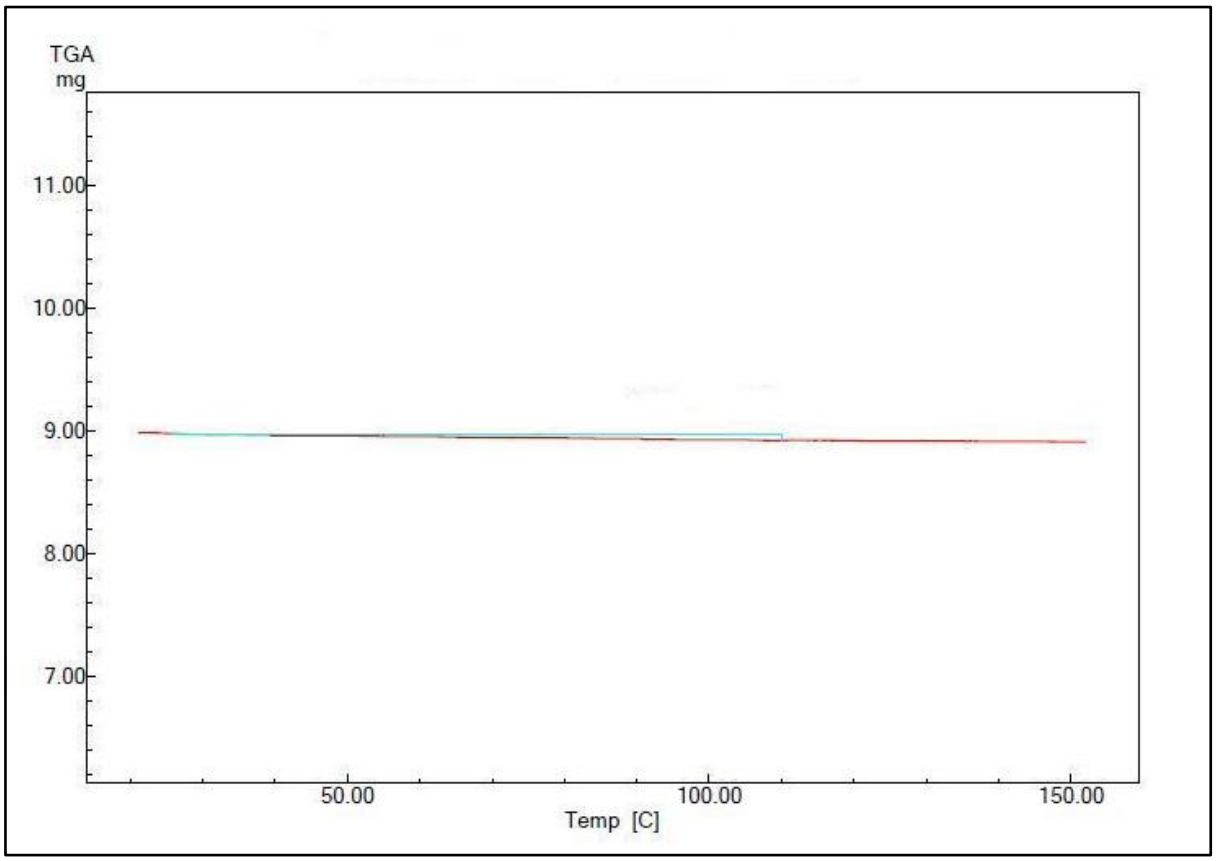

Figure 5.8 TGA thermogram of AZM-G indicating a weight loss of 0.61 %.

The TGA thermogram (Figure 5.8) illustrates the weight loss of amorphous AZM-G as a function of an increase in temperature. As indicated, the AZM-G sample only lost 0.61 % of its initial weight (Figure 5.8). According to the USP (2010) monograph for azithromycin, the percentage weight loss of a dihydrate and monohydrate after drying is 4.59 % and 2.30 %, respectively. Therefore, AZM-G could be characterised as being anhydrous. The TGA results, together with the Karl Fischer titration outcomes (Section 5.3.5) clearly indicated the absence of water molecules in the AZM-G structure. These results were congruent with the DSC findings of AZM-G, where it was established that the two endotherms that represented dehydration, as well as a crystalline melting event, were absent in the AZM-G sample. It was therefore concluded that the prepared AZM-G form was both anhydrous and amorphous.

5.3.5 Karl Fischer titration (KFT)

As depicted in Table 5.2, it was established with KFT that AZM-DH had a water content of 4.59 %, identical to the theoretical water content (4.59 %) representing a dihydrate, as per the USP (2010).

Table 5.2 Summary of the percentage water content of AZM-DH and AZM-G as determined with KFT and TGA

	Water content (%)	
	KFT	**TGA**
AZM-DH	4.59	4.40
AZM-G	0.61	0.61

The determined water content for AZM-G was 0.61 %. As discussed earlier, both the TGA and KF analyses confirmed the anhydrous state of AZM-G.

5.3.6 Microscopy

A normal HSM image (10x magnification at 25˚C) of AZM-DH is shown in Figure 5.9. Two SEM images of AZM-DH are further illustrated by Figure 5.10. These images illustrate the crystalline nature of AZM-DH. The prismatic habit of the crystalline AZM-DH was

characteristic and visible throughout these images. The melting point of 119.04˚C, as described in Section 5.3.3, was also verified with HSM, as the crystalline solids started to melt at 115˚C and were completely melted as the temperature was increased up to and past 119˚C.

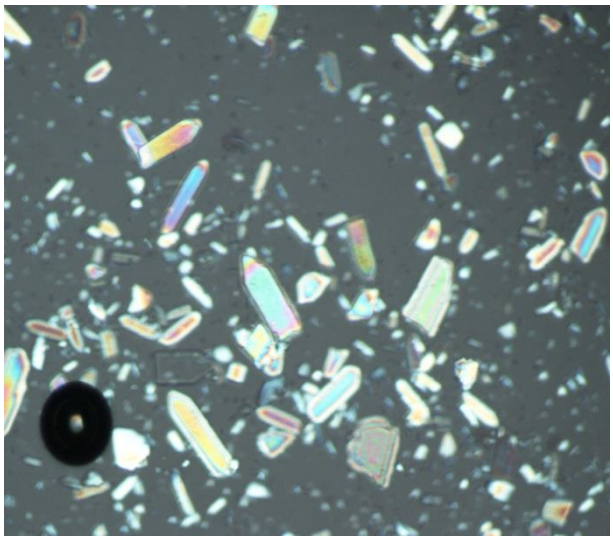

Figure 5.9 HSM image of AZM-DH (Temperature of 25˚C, Magnification at 10x, Sample covered with silicon oil).

The SEM images of AZM-DH (Figure 5.10) illustrated the morphology of this crystalline form. The AZM-DH particles in Figure 5.10a were examined on a scale of 500 µm, whereas the particles in Figure 5.10b were viewed on a scale of 200 µm. From these micrographs it is clear that AZM-DH showed a prismatic particle morphology.

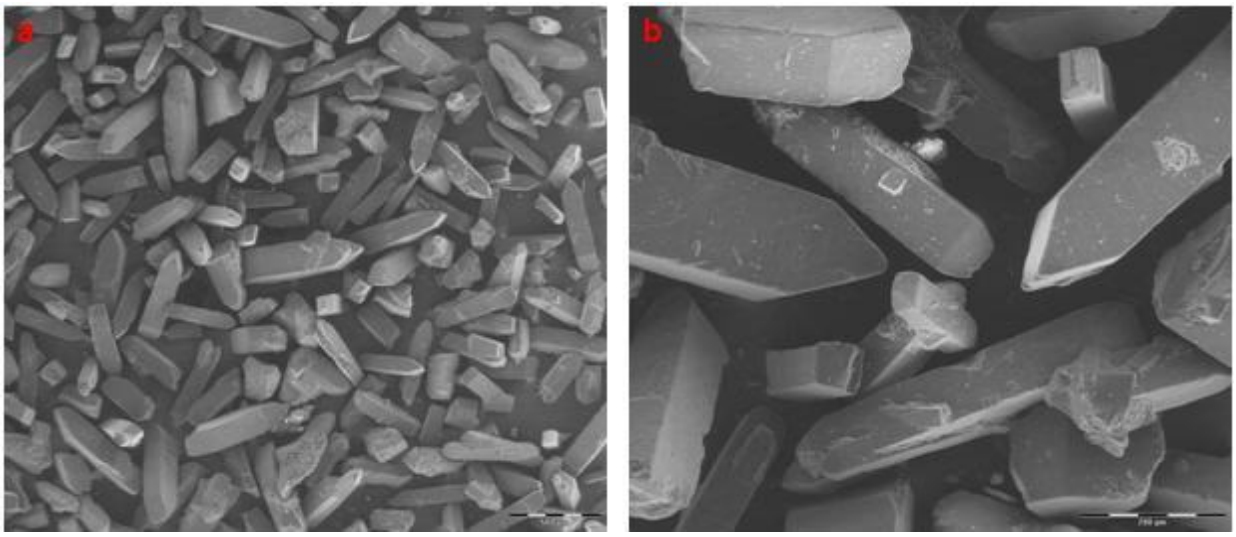

Figure 5.10 SEM images (a & b) of AZM-DH on a scale of 500 µm (a) and 200 µm (b).

The glassy nature of AZM-G (unmilled in its original glassy state) is visible on the HSM image presented in Figure 5.11a (10x magnification). Upon increasing the temperature, the AZM-G sample only displayed a morphological change at a temperature of 104˚C, where the solid glass transformed into a liquid state (Figure 5.13). This temperature corresponded well with the glass transition temperature *(T_g)* being obtained with DSC analysis (Section 5.3.3). The temperature was slowly increased up to 150˚C, where the AZM-G still presented as a glass-like liquid. No crystallisation of AZM-G into the structurally stable, crystalline AZM-DH, nor into AZM, was observed during HSM screening. As expected from all of the above data, no dehydration was observed with the HSM screening of AZM-G, therefore confirming the anhydrous state of glassy AZM.

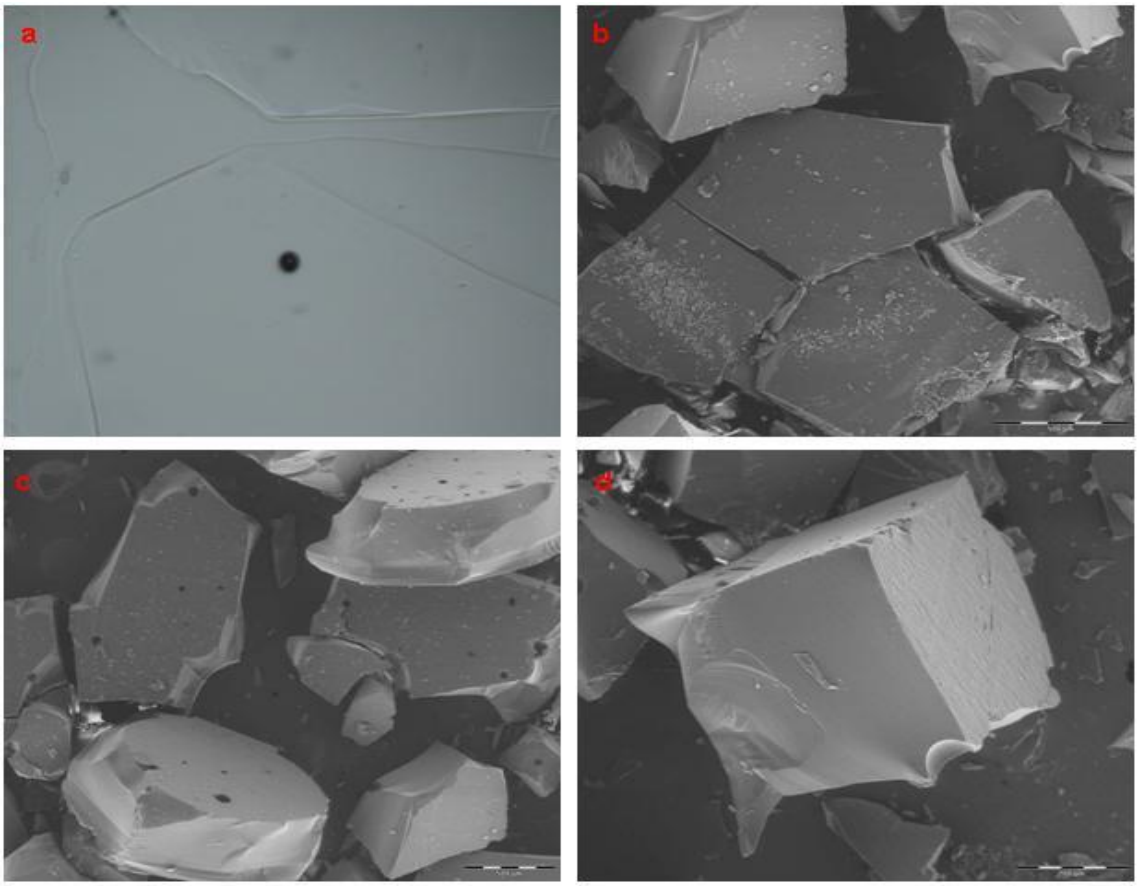

Figure 5.11 (a) HSM and (b-d) SEM images of unmilled AZM-G viewed on a scale of 500 µm (b-c) and 200 µm (d) respectively.

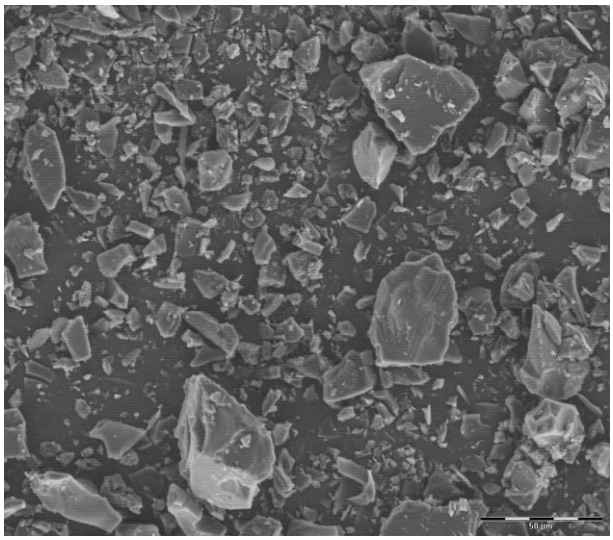

Figure 5.12 SEM image of milled AZM-G on a scale of 50 µm.

SEM images of unmilled, glassy AZM-G (Figure 5.11b-d) and of its milled state (Figure 5.12) were also taken. These images show the morphological glassy characteristics of AZM-G. Images displayed in Figure 5.11b-c were taken on a scale of 500 µm, whereas that in Figure 5.11d was taken at 200 µm. The increased energy that was coupled with the milling process could have caused structural, solid state changes, i.e. crystalline forms that transformed into amorphous forms, or amorphous forms that recrystallised back into the stable, crystalline state (Brittain & Fiese, 1999:334). As seen on the SEM images of the unmilled (Figure 5.11b-d) and milled (Figure 5.12) AZM-G samples, there were no morphological differences, nor any signs of recrystallisation due to the grinding process. This was indicative of a certain level of kinetic stability, which was of high significance to the bulk manufacturing of AZM-G. Because of the handling difficulty that unmilled AZM-G may have caused during product development, it was established that it would be best if AZM-G was milled into AZM-G powder. The AZM-G powder was later found to be much easier to handle than the unmilled AZM-G.

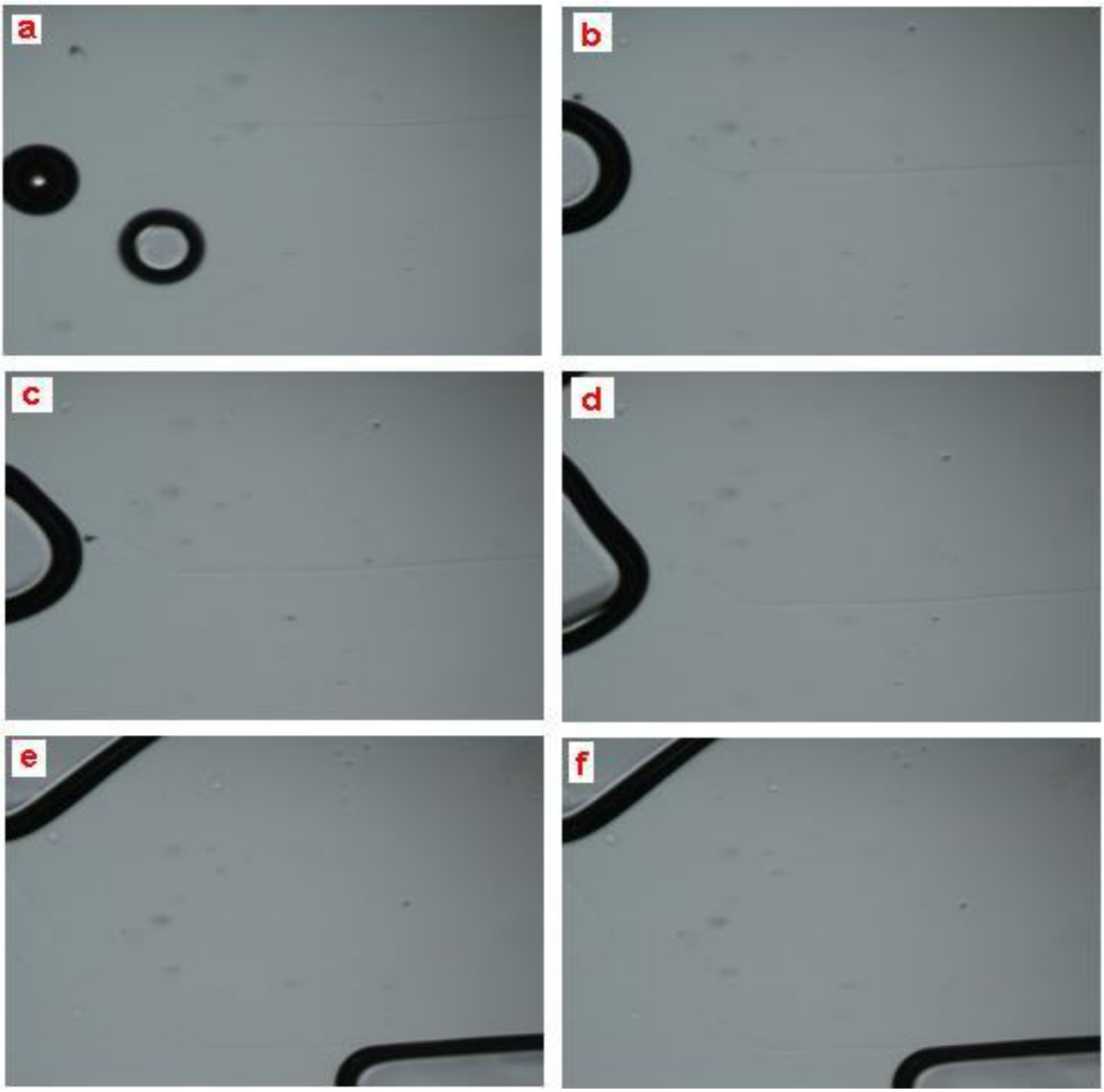

Figure 5.13 **Series of HSM images (a-f) of AZM-G illustrating the morphological changes during a glass transition from a solid glass into a liquid state. (a) HSM image taken at 80˚C illustrating that AZM-G is a glassy solid, (b) HSM image at 90˚C illustrating that AZM-G still exists as a glassy solid, (c) HSM image taken at 95˚C illustrating that the glassy solid is starting to show signs of reduced viscosity as the molecules become more mobile, (d) HSM image of AZM-G at 99˚C illustrating a further decrease in viscosity of the supercooled liquid (glass), (e) HSM image taken at 104˚C with the glass transition from the solid into the liquid being visible, (f) HSM image at 106˚C, illustrating the complete transition from the glassy solid into the liquid phase.**

5.4 Solubility of AZM-G

The four aqueous media being utilised to ultimately determine the solubility of AZM-G were phosphate buffer (pH 6.8), acetate buffer (pH 4.5), 0.1 M HCl (pH 1.2) and distilled water (BP, 2011). The materials and method that were used to perform the solubility study are described in Sections 2.4.3 and 2.4.4. AZM-DH was used as reference during this study, for comparing the unmilled and milled AZM-G samples with. Upon analysis of the solubility samples, results exceeding the concentration range of the HPLC method were obtained. It was much higher than anticipated, and hence not within the analytical range. Since solubility data is semi-quantitative, it was decided to accept the data 'as is' and not widen the analytical range. Extrapolation was utilised to ultimately quantify the samples exceeding the range.

5.4.1 Stability and solubility of azithromycin glass in 0.1 M HCl

It was previously stated that AZM shows improved acidic stability, in comparison with other macrolides, due to structural modification that results in a 15-membered lactone ring (Hoepelman & Schneider, 1995:146; Retsema & Fu, 2001:S4). The methyl-substituted nitrogen at position 9a of the aglycone ring is primarily responsible for blocking internal dehydration. This means that degradation of AZM mainly occurs *via* acid-catalysed hydrolysis of the ether bond, which ultimately results in the formation of the neutral cladinose sugar (Fiese & Steffen, 1990:39). Although AZM is more stable in an acid environment, it would still degrade. The difficulty in determining the solubility of different forms of AZM in such acidic environment is also discussed in this chapter. To establish the stability of AZM-G (with AZM-DH as reference) in acidic conditions, the study was performed with milled AZM-G according to the method being described in Section 2.6.2.

5.4.1.1 Results of acid stability

The degradation outcomes of the stability study in acidic conditions are illustrated in Figure 5.14. The onset of degradation was the same for AZM-DH and AZM-G, whilst similar percentages of degradation up until 90 minutes were achieved, where after AZM-G degraded at a slightly slower rate than AZM-DH. After 120 minutes, degradation resulted in 48.12 % and 45.89 % for AZM-DH and AZM-G, respectively (Figure 5.32).

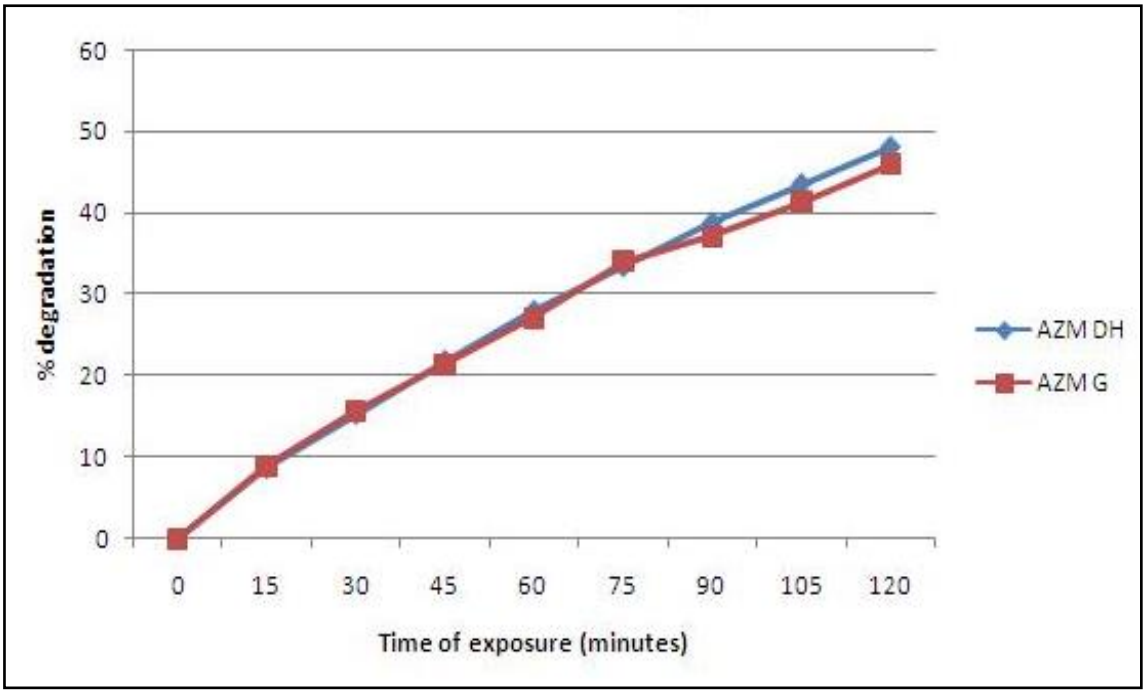

Figure 5.14 Percentage degradation of AZM-DH and AZM-G in 0.1 M HCl (pH 1.2).

This meant that almost 50 % of AZM-G degraded within 2 hours after being exposed to 0.1 M HCl (pH 1.2). In essence, since this condition could be applied to the conditions found within the human stomach, these findings may very well prove valuable to product development, in developing a solid dosage form (tablet or capsule) that would go through the stomach unchanged. This way the optimum concentration of AZM would be available for absorption, with the minimum (if any) altering effects, as a result of degradation.

This stability determination of AZM in 0.1 M HCl at pH 1.2 was performed with a fixed, small concentration of AZM (1 mg/mL) in 20 mL of 0.1 M HCl. This meant that the ratio of AZM to solvent favoured the solvent to a large extent, emphasising that more solvent was available to interact with the surface of the AZM particles. Fiese and Steffen (1990:39) determined that 10 % of AZM had degraded within 20 minutes at pH 2. They further established that the stability of AZM had improved by a factor 10 with every increase in pH unit (Fiese & Steffen, 1990:39). According to a stability study done by De Haro Moreno *et al*. (2009:225), AZM degraded within 6 hours in 0.1 M HCl, during which time it had lost all of its potency as an active drug.

In the following section, the solubility of AZM in 0.1 M HCl is discussed. During the solubility determination, the ratio of AZM to solvent favoured AZM, i.e. a supersaturated solution was prepared. Because of the ratio of AZM to solvent, the 0.1 M HCl present in this supersaturated solution was insufficient to cause complete degradation of AZM within

the 24 hour period. The degraded AZM was actively replaced by the excess AZM still present in the solution.

5.4.1.2 Solubility in pH 1.2

Although AZM is more acid-stable than the other macrolide antibiotics (Hoepelman & Schneider, 1995:146; Retsema & Fu, 2001:S4), it does degrade in an acidic environment (pH 1.2). Most marketed products of AZM are film-coated tablets to protect AZM from degradation in the stomach. These facts clearly indicated that the solubility determination of AZM in a low pH, aqueous medium would result in variable and inconsistent solubility values (Table 5.3).

Table 5.3 Solubility data of AZM in 0.1 M HCl

AZM-DH mg/mL	AZM-G (unmilled) mg/mL	AZM-G (milled) mg/mL
35.99 ± 0.82	35.99 ± 0.67	37.05 ± 0.25

With reference to Figure 5.15, it was established that AZM-DH achieved an average concentration of 35.99 mg/mL after 24 hours. AZM-G and AZM-G (milled) achieved average concentrations of 35.99 mg/mL and 37.05 mg/mL, respectively. The differences in solubility between AZM-DH and AZM-G (milled) related to an approximate increase of 3 %. The data in table 5.3 suggested that the solubilities of AZM-DH and AZM-G were identical, but that the solubility of the milled sample differed. The statistical p-value being calculated for AZM-DH and AZM-G (milled) was 0.0441, which could be considered as statistically significant (GraphPad software). These solubility values could only be considered as an indication of its solubility though, since the AZM starts degrading as soon as being exposed to such low pH conditions, and solvent mediated phase transformations could also occur within the solution (Sultana *et al*., 2006:100). Furthermore, the higher solubility value obtained for the milled sample could have been directly correlated with the particle size, since smaller particles have more contact with the solvent, compared to larger particles (Yalkowsky, 1999:87).

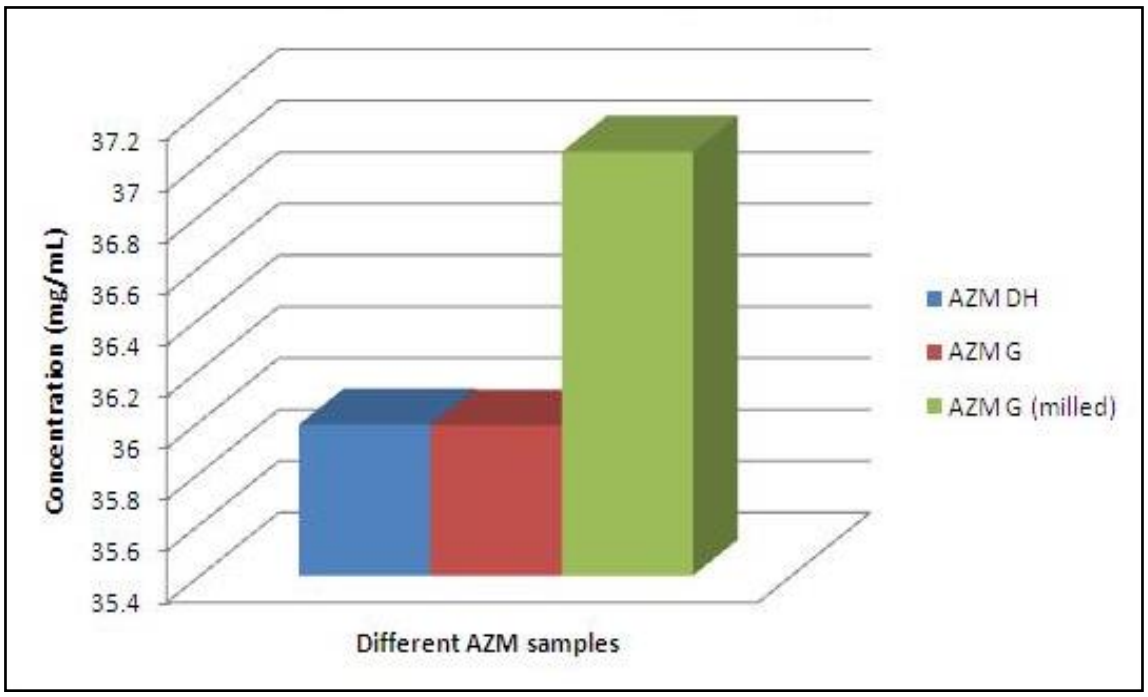

Figure 5.15 Histogram to compare the solubility values (mg/mL) obtained for AZM-DH, AZM-G and milled AZM-G in 0.1 M HCl (pH 1.2).

5.4.2 Solubility in acetate buffer (pH 4.5)

The solubility values of AZM-G in acetate buffer (pH 4.5) were almost identical to that of the reference, i.e. AZM-DH (Table 5.4). Figure 5.16 showed that milled AZM-G (11.40 mg/mL) was slightly more soluble (4.65 %) at pH 4.5 than AZM-DH (10.89 mg/mL). Unmilled AZM-G resulted in a final concentration of 10.80 mg/mL. The statistical p-value being calculated for the solubility values of AZM-DH and AZM-G (milled) was less than 0.0001, which could be considered extremely statistically significant (GraphPad software). This further confirmed that powdering (i.e. milled AZM-G) improved the solubility of the glass, due to a larger surface area exposure. No analysis was done on recovered samples after the solubility determination.

Table 5.4 Solubility data of AZM in acetate buffer (pH 4.5)

AZM DH mg/mL	AZM-G (unmilled) mg/mL	AZM-G (milled) mg/mL
10.89 ± 0.14	10.80 ± 0.16	11.40 ± 0.05

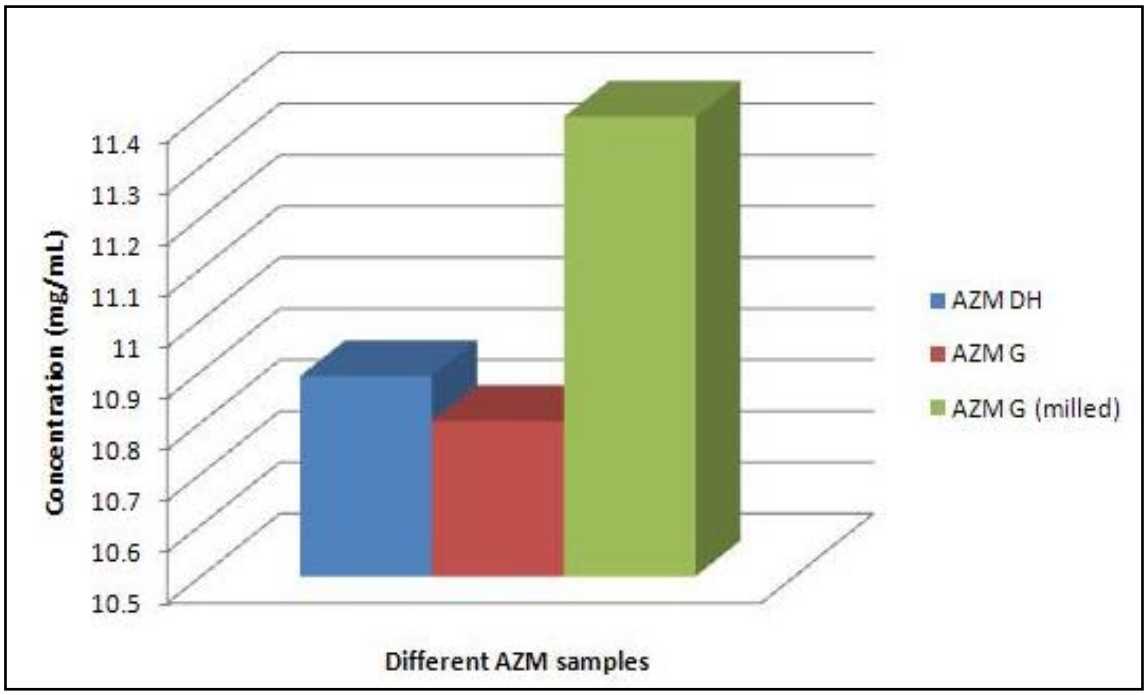

Figure 5.16 Histogram to compare the solubility values (mg/mL) obtained for AZM-DH, AZM-G and milled AZM-G in acetate buffer (pH 4.5).

5.4.3 Solubility in phosphate buffer (pH 6.8)

The data obtained during the solubility determination in phosphate buffer is summarised in Table 5.5. The solubility values being obtained for AZM-DH, AZM-G and AZM-G (milled) during this solubility study were 6.98, 9.01 and 9.70 mg/mL, respectively (Figure 5.17). With regards to the solubility of AZM-G (unmilled and milled), the results showed that the unmilled AZM-G was 29 % more soluble than AZM-DH. Milled AZM-G showed a 39 % improvement in solubility as a result of the smaller particles and the increased surface area being exposed to the solvent. The calculated p-value of the AZM-DH and the AZM-G (milled) was less than 0.0001, which was considered extremely statistically significant. With phosphate buffer as solvent, the conditions of the human small intestine were mimicked in terms of pH conditions. Since the pH of the human small intestine is above 6.0, this improved solubility could mean quicker dissolution rates and better absorption and

consequently an increase in the bioavailability percentage of the drug. No analysis was done on recovered samples after the solubility determination.

Table 5.5 Solubility data of AZM in phosphate buffer (pH 6.8)

AZM-DH mg/mL	AZM-G (unmilled) mg/mL	AZM-G (milled) mg/mL
6.98 ± 0.12	9.01 ± 0.06	9.70 ± 0.14

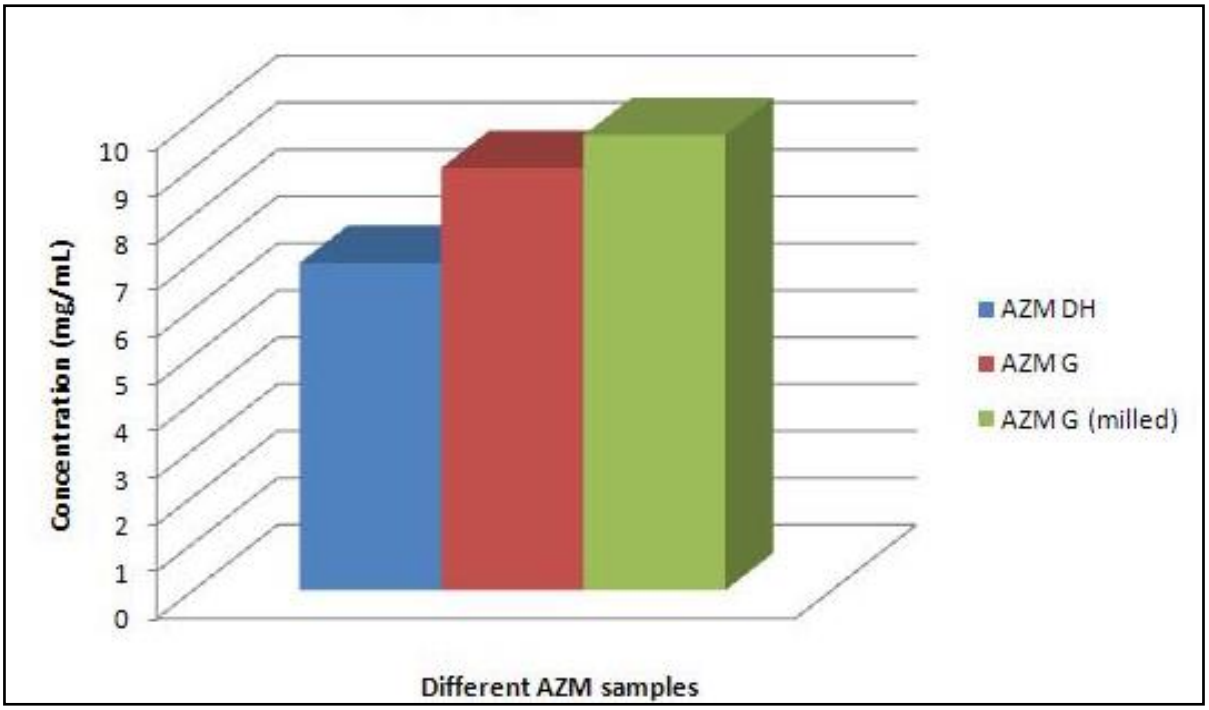

Figure 5.17 Histogram to compare the solubility values (mg/mL) obtained for AZM-DH, AZM-G and milled AZM-G in phosphate buffer (pH 6.8).

5.4.4 Solubility in water

The poor water solubility of AZM is considered problematic, in the sense that it influences other pharmacokinetic parameters to a large extent. The solubility outcomes in water showed that a very small amount of AZM-DH had dissolved at 37˚C after 24 hours of exposure (Table 5.6). The solubility of AZM-DH in water was determined as 0.07 mg/mL. The solubility of AZM-G (unmilled) was 0.30 mg/mL (Figure 5.18). This related to a 339 % improvement in the water solubility of AZM, as illustrated in Figure 5.18. The milled AZM-G showed a 328 % improvement in water solubility, with a concentration of 0.29 mg/mL. As mentioned earlier, an improvement in water solubility could also lead to

an increase in bioavailability, as a result of better absorption in the body. The calculated p-value for AZM-DH and the AZM-G (both unmilled and milled) was less than 0.0001, which was considered extremely statistically significant.

Table 5.6 Solubility data of AZM in water

AZM-DH mg/mL	AZM-G (unmilled) mg/mL	AZM-G (milled) mg/mL
0.07	0.30 ± 0.02	0.29 ± 0.02

Figure 5.18 Histogram to compare the solubility values (mg/mL) obtained for AZM-DH, AZM-G and milled AZM-G in distilled water.

The solubility in water was very low in comparison with the two buffers, but the highest difference and percentage improvement in solubility being achieved (Figure 5.19) was in water. The amorphous glass (milled or unmilled) showed a higher than 300 % increase in solubility compared to that of AZM-DH (Figure 5.19). Analysis results of recovered samples from water solubility will be discussed in Section 5.5.3.

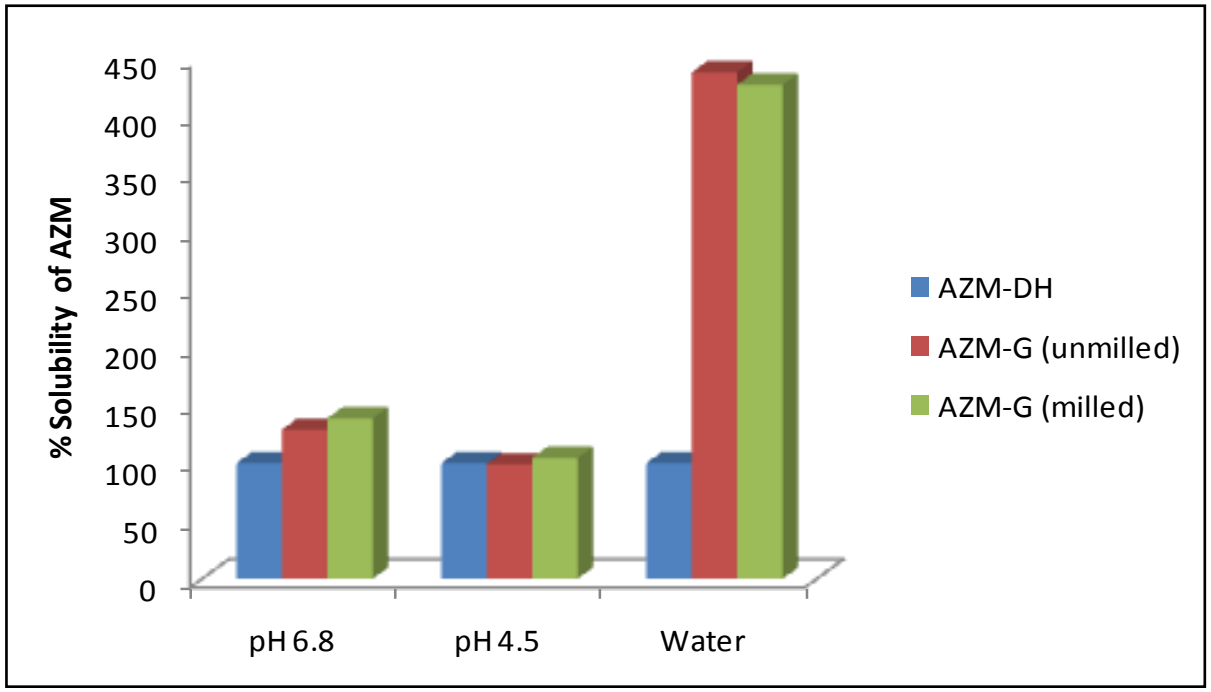

Figure 5.19 Comparative histogram of the solubility of AZM-DH (blue), unmilled AZM-G (maroon), and milled AZM-G (green) in different aqueous media having varying pH values.

5.5 Stability of AZM-G

In order to establish the stability of AZM-G, it was exposed to a high relative humidity (RH) and temperature, according to the method described in Section 2.5.1. AZM-DH was also included in this study to serve as reference and for indicating the possible instability of AZM-G. Vapour sorption and microcalorimetric tests were furthermore performed on the AZM-G sample.

5.5.1 Results

Moisture sorption analysis was performed, as described in Section 2.3.6, whilst the stability of the glass was monitored by means of microcalorimety (Section 2.3.5).

In order to determine the water vapour adsorption and desorption properties of AZM-DH and AZM-G (unmilled and milled), a relative humidity (RH) range of 0 % to 95 % was selected and executed at a constant temperature of 25˚C. The individual samples were dried at 50˚C (heating rate at 5˚C/min) for 60 minutes, as a standard pre-treatment, before commencing with the actual analysis.

The water vapour adsorption and desorption isotherms of AZM-DH are shown in Figure 5.20. The weight of the AZM-DH sample increased by 1.37 % after conditions of 95 % RH were reached, where after the RH was gradually decreased to 2.37 % RH. This decrease in RH resulted in the weight of the AZM-DH sample dropping from 1.37 % (95 % RH) to 0.56 % (2 % RH). The adsorption isotherm (Figure 5.20) displayed a rapid increase in weight percentage from approximately 6 % RH up to about 15 % RH, where after the adsorption gradually increased at a slow rate, until reaching a limiting value at 90 % RH. This adsorption isotherm of AZM-DH could be characterised as a Type Ib isotherm. It could also be referred to as a Langmuir-type isotherm. This type of isotherm is limited to a monolayer of adsorbed vapour/water. The surface area being calculated for AZM-DH during this test was 4.44 m^2/g. According to Hameed *et al*. (2006:822), the essential characteristics of the Langmuir isotherm can be expressed in terms of a dimensionless equilibrium parameter (R_L). This parameter is defined by the following:

$$R_L = 1 / (1+b_L.C_0) \qquad (5.1)$$

Where: *b* represents the Langmuir constant and C_0 the initial concentration of AZM.

In the event that $R_L > 1$, the isotherm is regarded as unfavourable for adsorption, whereas if $R_L = 1$, the isotherm is linear, whilst if $R_L = 0$, then the isotherm is irreversible and if $0 < R_L < 1$, then the isotherm is favourable for adsorption. The R_L value for AZM-DH was calculated as 0.55, according to which AZM-DH was thus favourable for adsorption (Ramachandran *et al*., 2011:23).

The adsorption/desorption isotherms of AZM-G (unmilled) are illustrated in Figure 5.21. Up until a 10 % RH, the AZM-G sample weight remained unchanged. At a 15 % RH a weight increase was recorded (0.06 %), where after the weight of AZM-G increased to 3.85 % at 95 % RH. Desorption mimicked the shape of the adsorption curve and the weight gradually dropped, resulting in a weight of 0.70 % at 5 % RH. The adsorption curve could be described as a Type III isotherm. This type of isotherm is associated with a monolayer forming on the surfaces of those areas of the solid that exhibit the most activity. As the amount of vapour/water increases, the most active sites are packed with layers of vapour/water, instead of a monolayer forming over the complete surface of the solid. The surface area being calculated for AZM-G (unmilled) during this experiment was 1.54 m^2/g. This surface area was an estimated area only, because the BET (Stephen Brunauer, Paul Emmett, Edward Teller) method for calculating the surface area actually is not applicable to Type III isotherms. The R_L value for AZM-G was calculated as 0.99, indicating that

AZM-G was favourable for adsorption, although it was very close to being submissive to linear adsorption (Hameed *et al*., 2006:822).

Figure 5.22 represents the adsorption/desorption isotherms of AZM-G (milled). The weight of milled AZM-G only started to increase after the RH had reached about 10 %. This gradual increase in weight was coupled with the increase in RH (up to 95 %). An adsorption weight increase of 5.14 % was recorded at 95 % RH. The desorption isotherm was almost identical to the adsorption isotherm. The decrease in RH resulted in a weight loss for AZM-G (milled) from 5.14 % (at 95 % RH) to 0.21 % at 0 % RH. The adsorption isotherm for AZM-G (milled) could also be described as a Type III isotherm, thus correlating well with the isotherms being achieved with the unmilled AZM-G. The surface area of AZM-G (milled) during this experiment was calculated as 1.83 m^2/g. As with unmilled AZM-G, this surface area of the milled AZM-G was an estimated area, because of the BET method for calculating the surface area not actually being applicable to Type III isotherms. The R_L value for milled AZM-G was calculated and found to be exactly 1. This indicated that AZM-G was subdued to linear adsorption (Hameed *et al*., 2006:822).

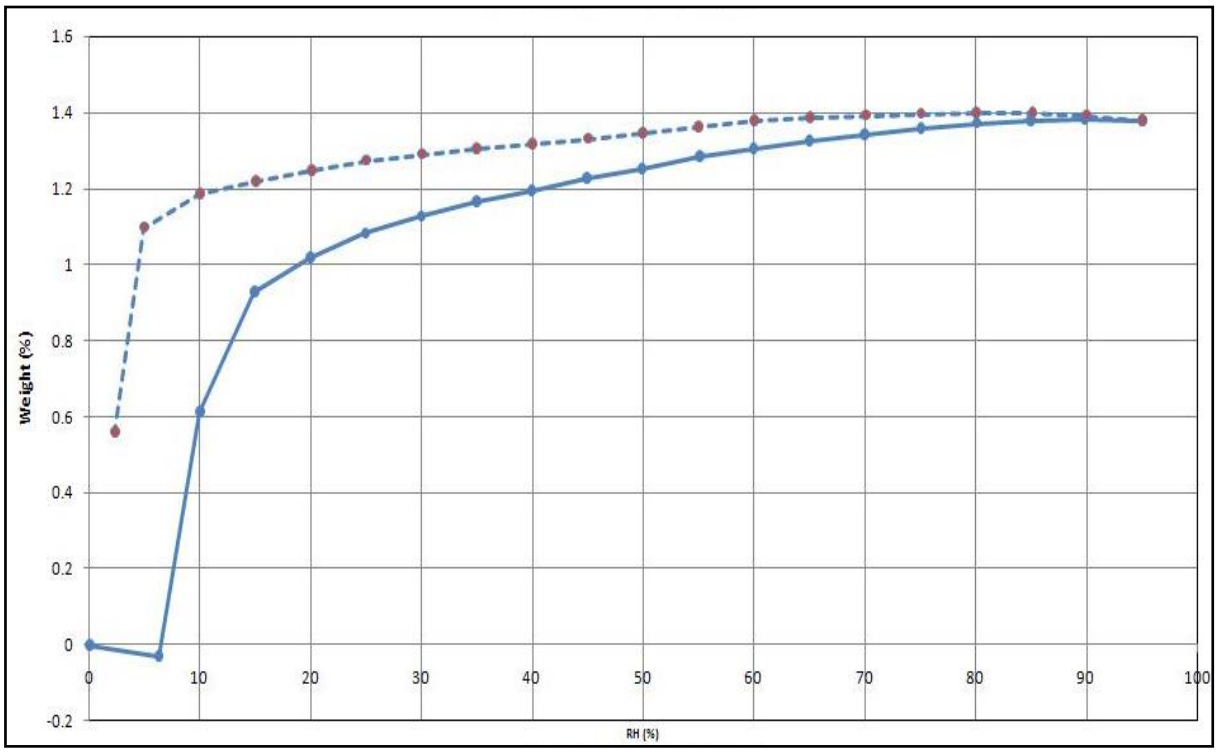

Figure 5.20 Water vapour adsorption (solid line) and desorption (dotted line) isotherms of AZM-DH (x-axis representing the % RH, y-axis representing the % weight).

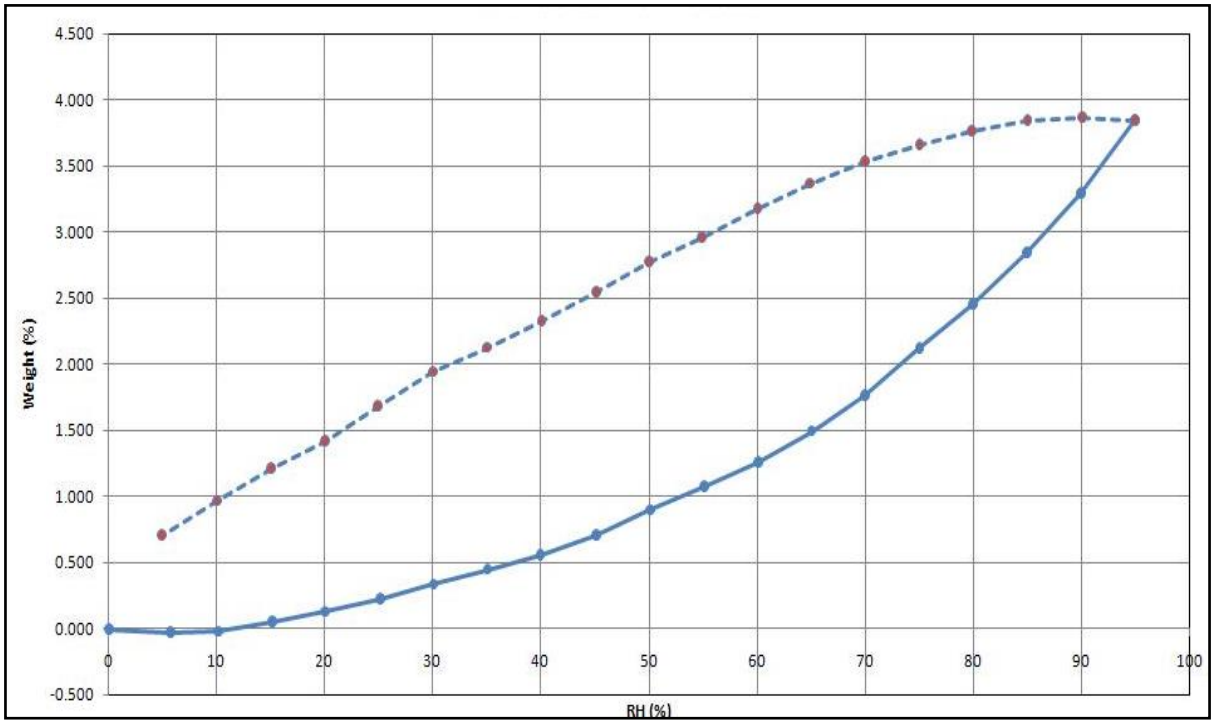

Figure 5.21 Water vapour adsorption (solid line) and desorption (dotted line) isotherms of unmilled AZM-G.

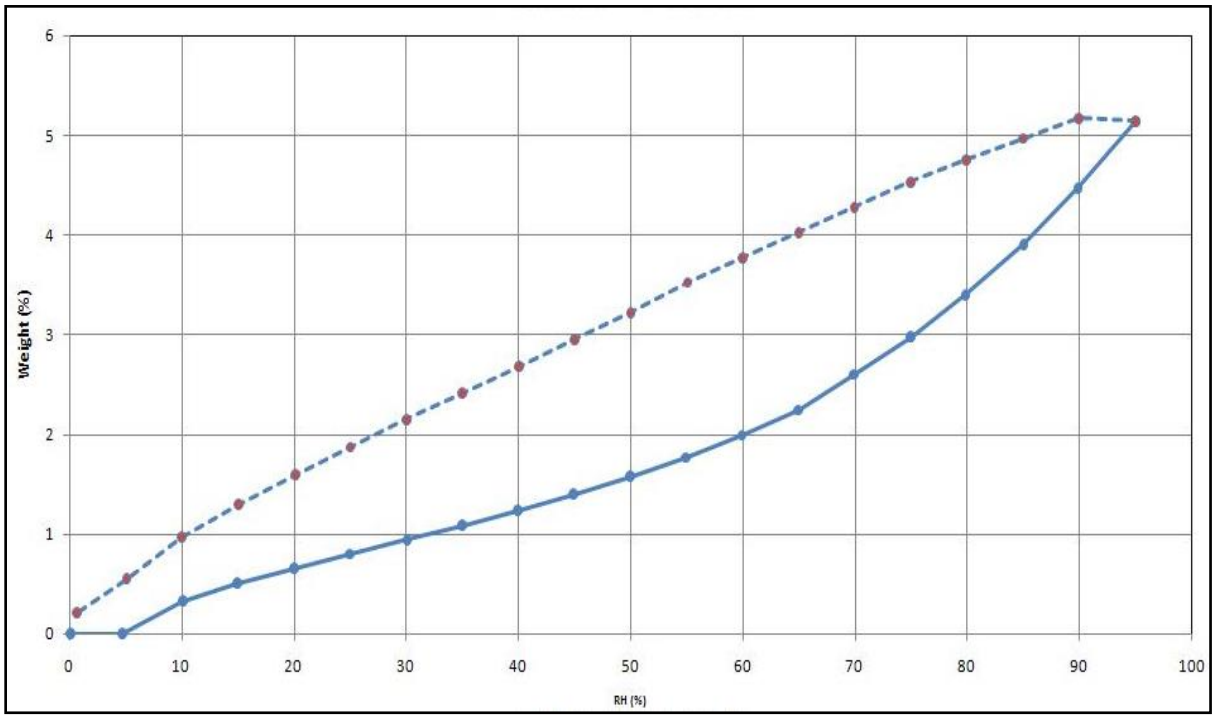

Figure 5.22 Water vapour adsorption (solid line) and desorption (dotted line) isotherms of milled AZM-G.

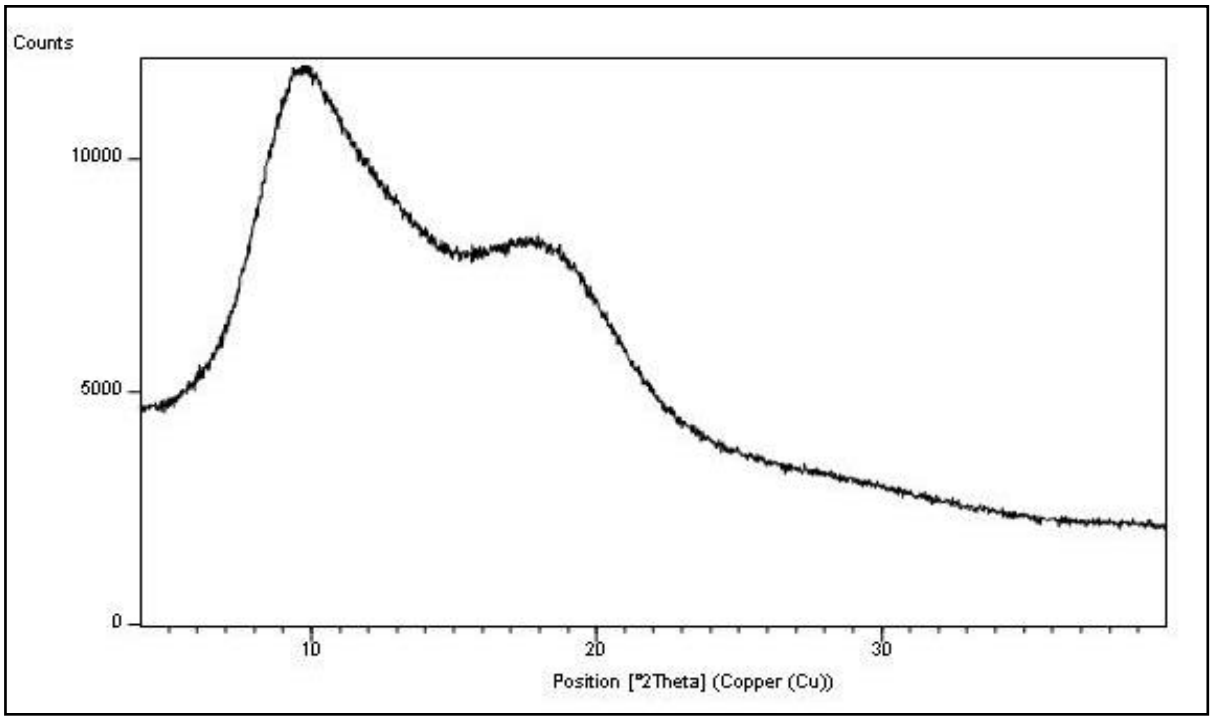

Figure 5.23 XRPD pattern of AZM-G after exposure to 100 % RH for a period of 3 days.

The stability of AZM-G (milled) in conditions relating to 100 % RH was proven by exposing AZM-G to such conditions in a microcalorimeter. The sample was then removed and analysed using XRPD. The XRPD pattern obtained is illustrated in Figure 5.23 and shows the typical halo pattern that represents amorphous solids, as described in Section 5.3.2. It was hence established that AZM-G (milled) was indeed extremely stable, when exposed to moisture (100 % RH for 3 days) and that humidity had no inducing effect on its transition into the crystalline state. In essence, the moisture adsorption/desorption isotherms, together with the XRPD pattern, clearly emphasised the extremely desirable and unique stability of this glassy form of AZM.

5.5.2 Stability study

The results from the various screening tests are summarised in Table 5.7. These results reflect the stability at conditions of 40°C and 75 % RH. The melting point (T_m) of AZM-DH, the glass transition temperature (T_g) of AZM-G, the percentage weight loss (%) and the percentage water (% H_2O) present in each sample were determined by DSC, TGA and KFT, respectively (Table 5.7). The FTIR spectrum of AZM-DH was used as a standard reference for comparison against the FTIR spectra of the weekly analysed AZM-G (unmilled) samples. As seen in Table 5.7, the FTIR spectra generated over the duration of

the stability study were demonstrative of an anhydrous form of azithromycin. HSM was performed to verify the results obtained from the DSC and to capture visual images of the morphological changes during the heating process, as well as to identify possible phase transitions resulting from exposure to heat. The dehydration of AZM-DH was clearly visible during the HSM screening.

Table 5.7 Summary of the screening test outcomes of AZM-G during the four weeks stability study at 40°C and 75 % RH

Analysis	Week 0	Week 1	Week 2	Week 3	Week 4
DSC: T_g(˚C) (mid-point)	108.68	107.54	105.88	106.57	107.12
TGA: (%)	0.98	5.06	4.21	4.22	4.01
KFT: (% H_2O)	0.61	3.45	3.17	3.13	3.22
XRPD	Amorphous	Amorphous	Amorphous	Amorphous	Amorphous
FTIR	Anhydrous	Anhydrous	Anhydrous	Anhydrous	Anhydrous
HSM	√	√	√	√	√

5.5.2.1 DSC analyses of AZM-G from weeks 0 - 4.

As a guideline and reference, AZM-DH was also exposed to the above conditions for four weeks. Since AZM-DH has been proven to be the stable, solid state form of azithromycin (Gandhi *et al*., 2002:183), the DSC analyses of AZM-DH were only done at weeks 0 (initial), 2 and 4 (Figure 5.24).

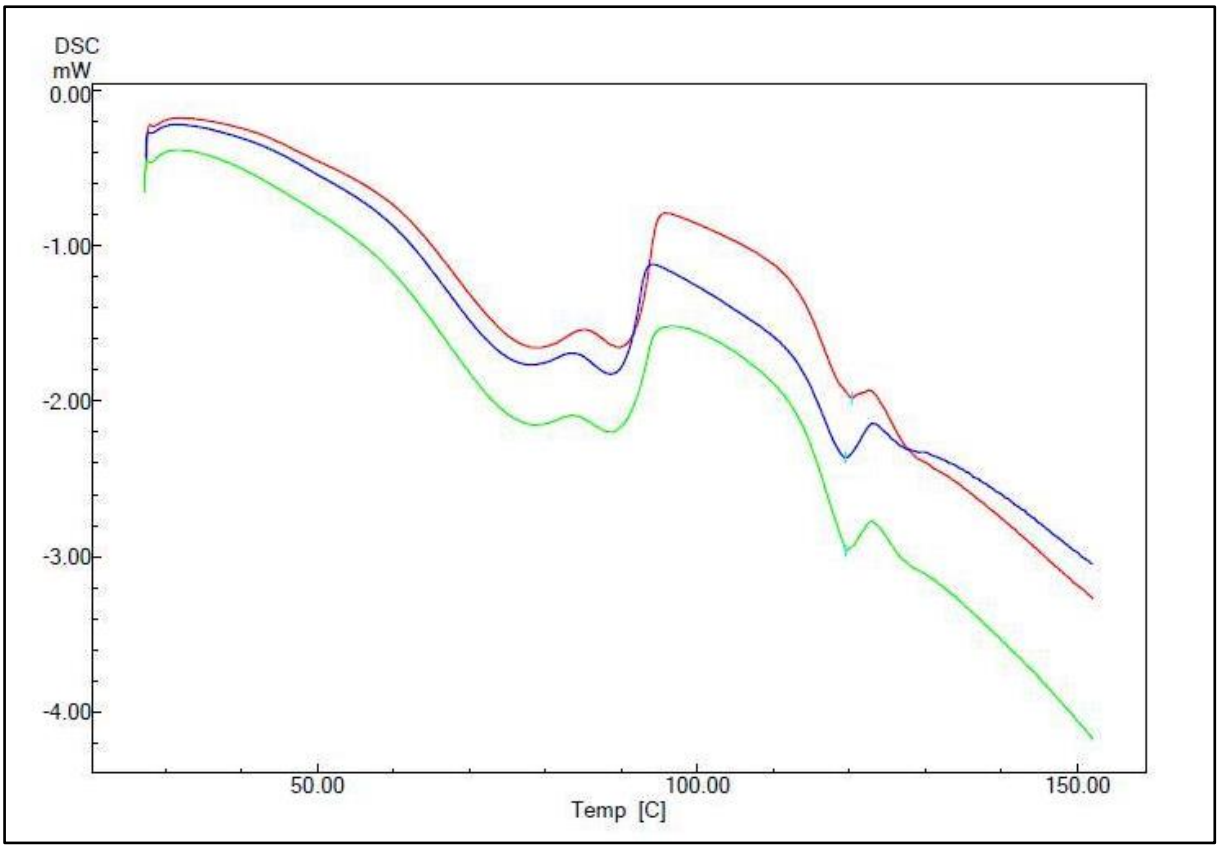

Figure 5.24 Overlay of DSC traces of AZM-DH generated during the stability study (Initial (blue), Week 2 (green), Week 4 (red)).

The respective melting points of AZM-DH during weeks 0, 2 and 4 were 119.46˚C, 119.59˚C and 120.38˚C, respectively (Figure 5.24). These DSC traces correlated well with the DSC thermogram, obtained during the characterisation of AZM-DH (Section 5.3.3, Figure 5.5).

Table 5.8 T_g values of AZM-G according to various formulae

	% water	Linear (K)	Gordon-Taylor (K)	Fox (K)	Experimental (K)
Initial	0.61	381.33	377.91	378.65	382.83
Week 1	3.45	373.03	355.72	359.50	381.69
Week 2	3.17	372.30	356.29	359.61	380.03
Week 3	3.13	373.07	357.16	360.45	380.72
Week 4	3.22	373.38	356.99	360.38	381.27

The T_g for the AZM-G samples being analysed during the fourth week of stability testing ranged between 380.03 - 382.83 K (approximately 105 - 109˚C). Usually, amorphous solids exhibit the tendency to absorb moisture in large quantities (Hancock & Zografi, 1997:7; Hancock & Zografi, 1994:471). The presence of water causes an increase in molecular mobility and can ultimately negatively impact on the physical stability of AZM-G (Chawla & Bansal, 2009:696). Consequently, this plasticising effect lowers the T_g of AZM-G (Zografi & Hancock, 1993:412). The effect of water as plasticiser can also be described and predicted by three different formulae, i.e. the Linear-, the Gordon-Taylor- and the Fox equations (Hancock & Zografi, 1997:4).

The **Linear** equation is used to calculate the T_g of a mixture and can be described as:

$$T_{g\,mix} = w_1 T_{g1} + w_2 T_{g2} \qquad (5.2)$$

Where: w is the weight fraction of each component of the mixture, T_{g1} and T_{g2} are the glass transition temperatures (in Kelvin) of the components of the mixture.

The **Gordon-Taylor** equation is the most popular equation used to calculate the T_g of the mixture. It can be expressed as (Hancock & Zografi, 1997:4):

$$T_{g\,mix} = \frac{(w1Tg1 + kw2Tg2)}{(w1 + kw2)} \qquad (5.3)$$

Where: $k = \frac{(\rho 1 Tg1)}{(\rho 2 Tg2)}$

ρ is the respective density of each component within the mixture. The density of AZM being used was ρ = 1.18 g/cm^3.

The **Fox** equation is used when the densities of the respective components are equal. This equation is expressed as (Hancock & Zografi, 1994:472):

$$\frac{1}{Tgmix} = \frac{w1}{Tg1} + \frac{w2}{Tg2} \qquad (5.4)$$

However, the lowering in T_g, as expressed by the experimental values in Table 5.8, indicated that the plasticising effect was minimal to almost none. According to the predictions using the Linear-, the Gordon-Taylor- and the Fox equations, the stability of AZM-G was furthermore emphasised when comparing those results with the actual experimental T_g results. From the values showed in Table 5.8 it is clear that the influence of water on AZM-G did not follow the expected lowering in T_g. From the data it became

clear that the relationship between water and AZM-G did not fit the predicted relationships, as calculated using the three said equations. This showed that, although AZM-G adsorbed a significant amount of water during exposure to relatively high humidity conditions, this amount of water was still not enough to have a significant plasticising effect.

Also, this phase transition was not preceded by the two endotherms, as was evident for AZM-DH. The absence of dehydration peaks in all of the AZM-G samples used in this study (Figures 5.24 and 5.25), indicated that there was no structurally bound water present. As mentioned, anhydrous azithromycin has the ability to absorb moisture fairly easily in order to convert into the more stable, hydrated forms. Because of the hygroscopic nature of azithromycin, the logical passage for an unstable anhydrate would be to quickly convert into a higher hydrated and more stable, hydrated form (Gandhi et al., 2002:181).

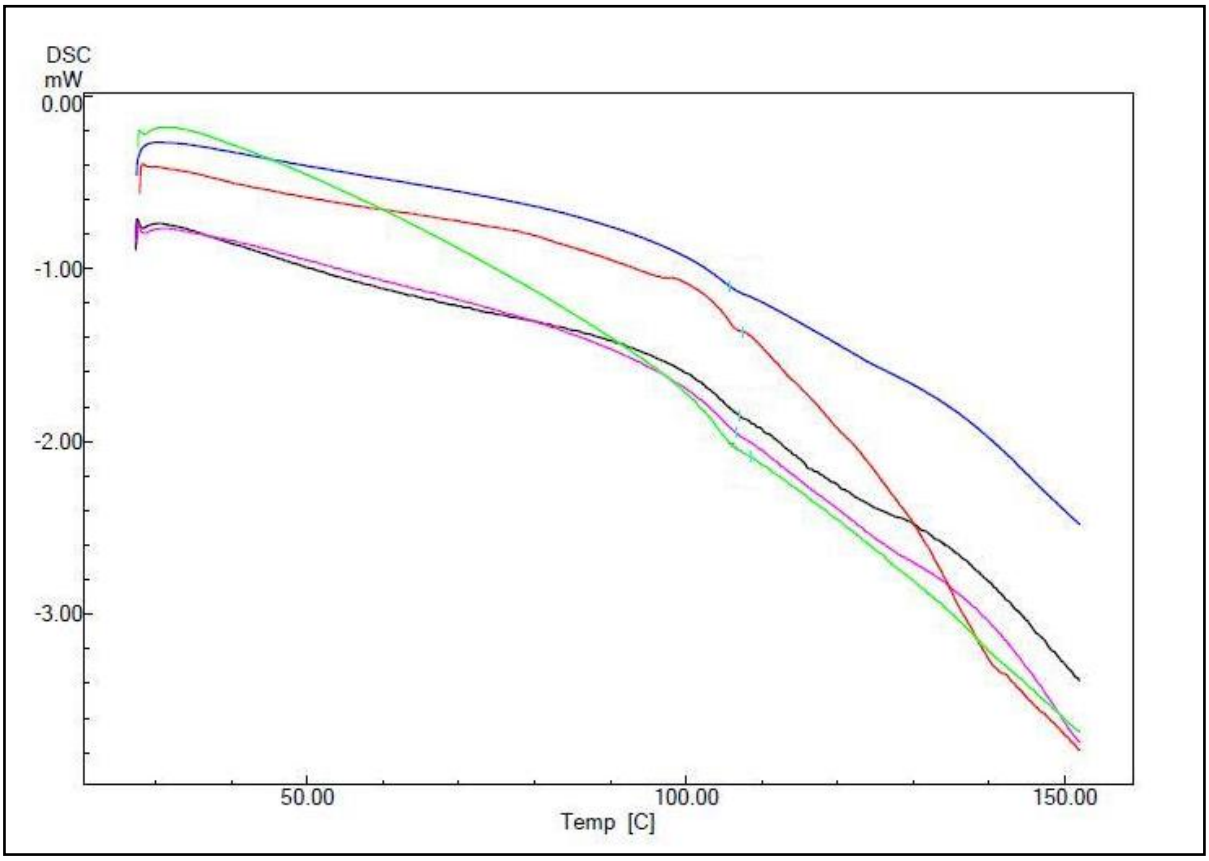

Figure 5.25 Overlay of DSC traces of AZM-G generated during the stability study (Initial (green), Week 1 (red), Week 2 (blue), Week 3 (magenta), Week 4 (black)).

In the presence of water, the anhydrate will first convert into the monohydrate, where after the monohydrate will ultimately transfer into the chemically stable dihydrate. For AZM-DH, two dehydration peaks can be seen in Figure 5.24 between 70˚C and 100˚C. Those dehydration peaks were absent in all of the AZM-G samples, as illustrated by the results obtained during DSC analyses (Figure 5.25). Thus, according to the DSC results being generated, it could be stated that AZM-G (unmilled) remained stable in its amorphous solid state (due to the T_g and the absence of a crystalline melt) for the duration of the stability study, and hence have a weak tendency (compared to other anhydrates and amorphous forms) to transform to the dihydrate crystal form.

5.5.2.2 TGA results for AZM-G during stability study

When AZM (dihydrate or monohydrate) is exposed to high enough temperatures to initiate the dehydration process, a theoretical weight loss value is given for the amount of water molecules being lost with drying within a certain temperature range. For AZM-DH, this theoretical weight loss value is 4.59 %, whereas the monohydrate theoretically presents with a 2.30 % weight loss (Gandhi *et al*., 2002:179). According to USP (2010) guidelines, some monohydrates present with a 4.0 - 6.50 % weight loss after being dried (USP, 2010). For hydrates, it is best to analyse with TGA in conjunction with Karl Fischer titration (KFT). With these two screening tests, the exact water content (bound or adsorbed on the surface) of the sample was determined during this study.

Correlation between the TGA and KFT screening results was a clear indication of the hydrated state of the azithromycin samples. Removal time from the storage conditions to analyse the samples in the laboratory was kept to a very short time. Upon arrival in the laboratory, analysis was commenced immediately. The initial analysis of AZM-DH resulted in a 4.88 % weight loss. The TGA results for weeks 2 and 4 showed a sample weight loss of 5.14 % and 5.67 %, respectively (Figure 5.26). This indicated an increase in weight loss over time of exposure to the stability conditions. With reference to the KFT results, as discussed in Section 5.5.2.3, it could be concluded that AZM-DH was the most stable form of AZM and that the increased weight loss achieved with TGA was due to the evaporation of adsorbed water on the surface of AZM-DH.

It is common for crystalline solids to adsorb small amounts of moisture on their surfaces. In the event of a large amount of moisture being adsorbed, the crystalline solid may transform into a hydrate/higher level hydrate (Hancock & Zografi, 1997:7). This adsorbed water was previously discussed and the isotherm for AZM-DH was characterised as a

Type Ib isotherm. It could also be referred to as a Langmuir-type isotherm. This type of isotherm is limited to a monolayer of adsorbed vapour/water (Hameed *et al*., 2006:821; Rouquerol *et al*., 1999:440). The vapour sorption results during this study showed that AZM-DH adsorbed 1.36 % of moisture at 75 % RH. Combining this percentage of adsorbed moisture at 75 % RH with the water content, as determined by KFT, it correlated well with the weight loss being indicated by the TGA result. A weight loss relating to the TGA results could thus be expected for AZM-DH with exposure to 75 % RH.

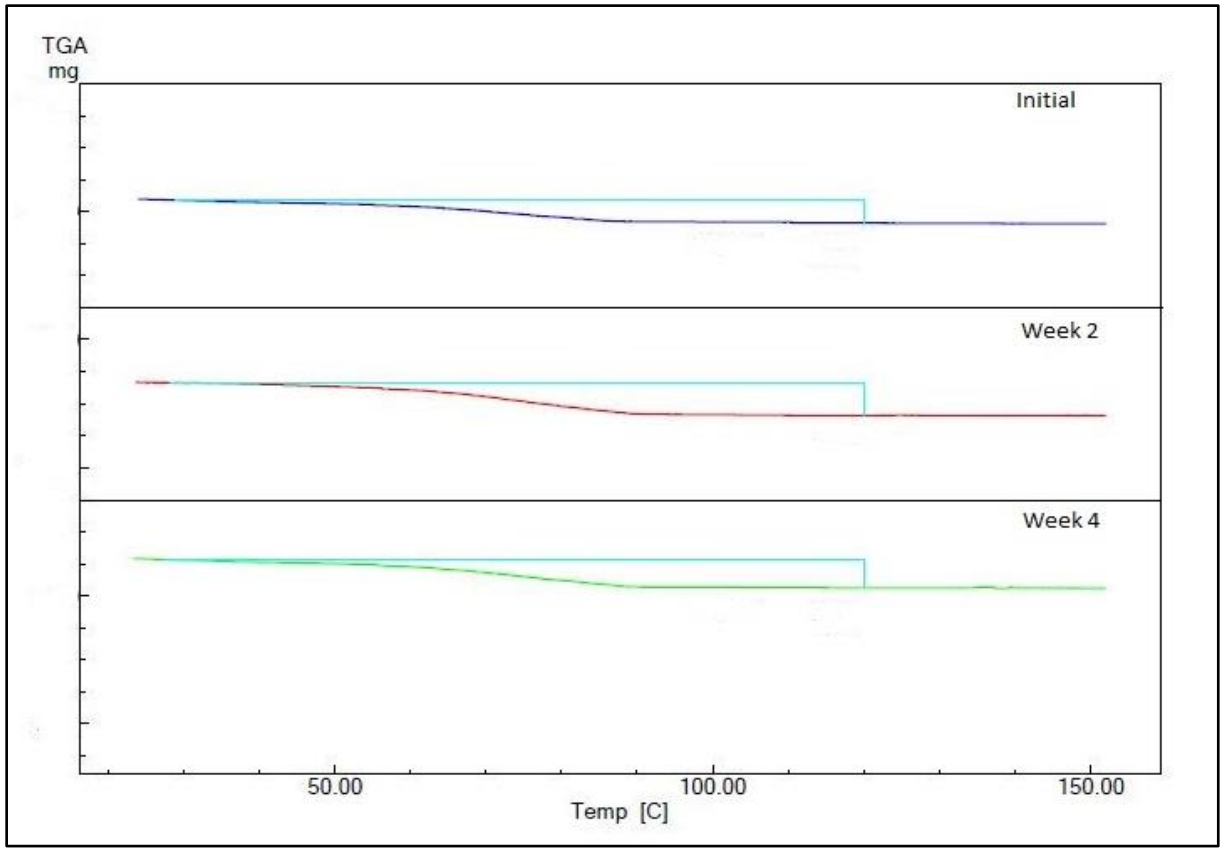

Figure 5.26 Overlay of TGA thermograms of AZM-DH generated during the stability study (Initial (blue), Week 2 (red), Week 4 (green)).

With reference to Figure 5.27, the TGA screening results indicated the percentage weight loss of each AZM-G sample being analysed weekly. The initial AZM-G sample showed an insignificant weight loss of less than 1 %. After a week, a significant weight loss was observed. The water (according to KFT) present in the samples were adsorbed moisture on the surface of the AZM-G particles (refer to vapour sorption results as described in Section 5.5.1). The water hence formed a monolayer on the surface of AZM-G. As mentioned earlier, the amount of adsorbed moisture on AZM-G represented a weight

increase percentage of 2.15 % at 75 % RH. Therefore, the moisture was not as such bound to the structure, nor was it an intrinsic part of each drug molecule.

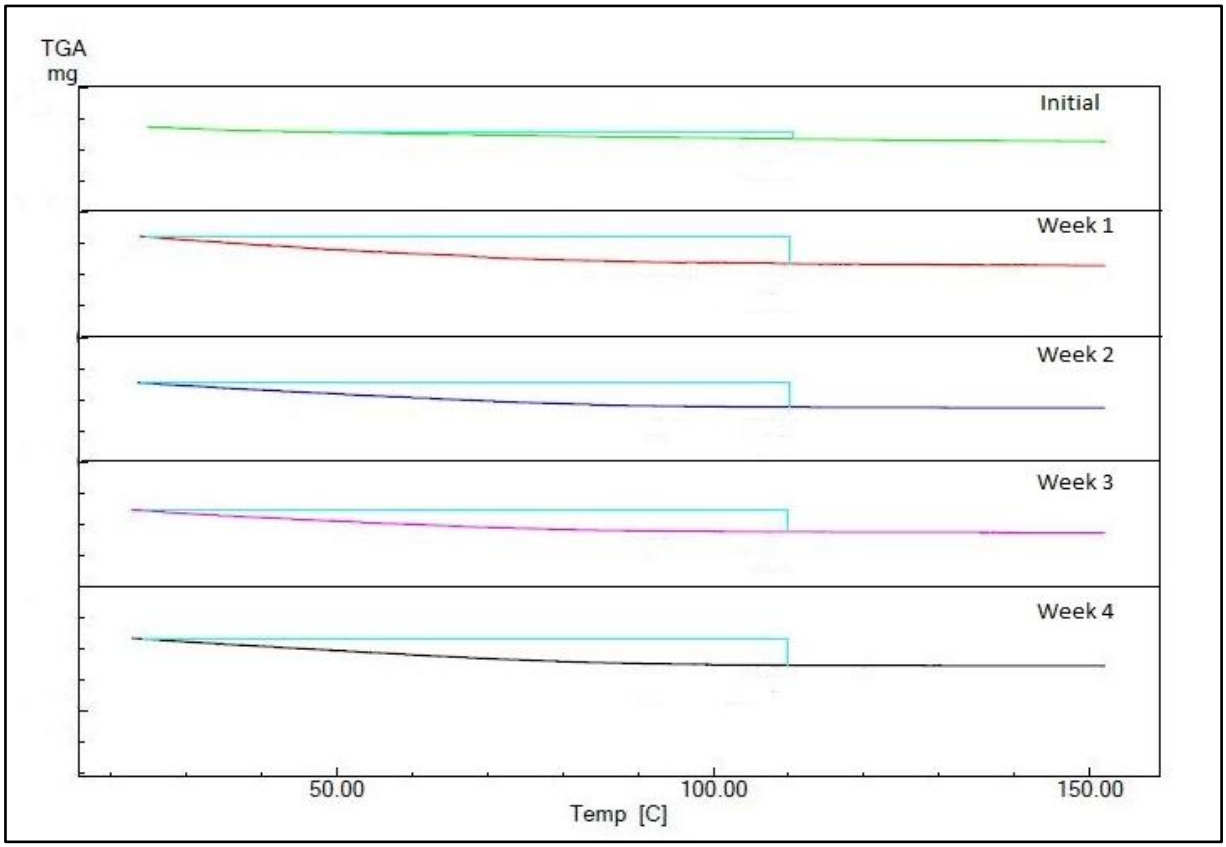

Figure 5.27 Overlay of TGA thermograms of AZM-G generated during the stability study (Initial (green), Week 1 (red), Week 2 (blue), Week 3 (magenta), Week 4 (black)).

5.5.2.3 KFT results

Karl Fischer titration (KFT) is a technique used to determine the percentage water content of a given sample. The water content of the initial AZM-DH sample was determined for use as a standard reference for identifying the expected uptake of water by the anhydrous glass samples. The AZM-G (unmilled) samples were carefully removed from the temperature- and humidity controlled chamber and placed in desiccators (at ambient temperature) to avoid unnecessary exposure to environmental conditions. Each sample was weighed (in a tight-sealed glass weighing boat) before analysis on the KFT in duplicate.

The water content of AZM-DH was measured as 4.58 % and 4.51 %. The initial AZM-G samples showed water contents of 0.62 % and 0.52 %. After a week of exposure to the

stability testing conditions, KFT results were more than 3 % for AZM-G. For the rest of the stability testing period, the water content remained stable at 3.0 - 3.50 %. The increased water content, however, had no impact on the structural stability of the glass. DSC results also emphasised the structural stability of the glass, since all DSC traces of AZM-G showed a T_g. The vapour sorption results, as discussed in Section 5.5.1, demonstrated that water was only adsorbed on the surface of AZM-G and that it had no effect on the structural stability of AZM-G. It was also determined that AZM-G was only favourable for adsorption of moisture/water, without water having any effect of recrystallisation on AZM-G.

5.5.2.4 XRPD results

AZM-DH is the stable, solid state form of azithromycin (Gandhi *et al*., 2002:183). The initial XRPD pattern for the dihydrate showed characteristic peaks with good intensities, indicative of the crystalline state of AZM-DH (Figure 5.28) (Gandhi *et al*., 2002:183). This exact pattern with its characteristic peaks was maintained by the dihydrate throughout the four weeks of exposure to the stability testing conditions, thereby thus confirming the stability of the dihydrated state of AZM. XRPD analysis of the initial AZM-G (unmilled) sample resulted in no peaks, but only in a typical halo pattern, indicative of amorphicity (Chieng *et al*., 2011:620; Yu *et al*., 1998:124). Throughout the four-week study, the XRPD results gave no indication of recrystallisation into the known, stable, dihydrated crystalline form (Figure 5.29), hence signifying the stability of AZM-G, even upon exposure to a high relative humidity of 75 %.

These XRPD patterns also clarified the structural uncertainties that arose during KFT analysis (Section 5.5.2.3). If the water content of more than 3 % was structurally bound, the amorphous solid would have changed and become crystalline, due to sufficiently increased molecular mobility and would the product hence be classified as a hydrate (Yu, 2001:32). This water could have acted as a plasticiser and cause the phase transformation from amorphous to crystalline (Yu, 2001:33). The conversion into the stable, crystalline form would have resulted in peaks showing on the XRPD pattern at different scattering angles. The halo type XRPD pattern of AZM-G (Figure 5.29) would have changed and resulted in a pattern equal to that of AZM-DH (Figure 5.28).

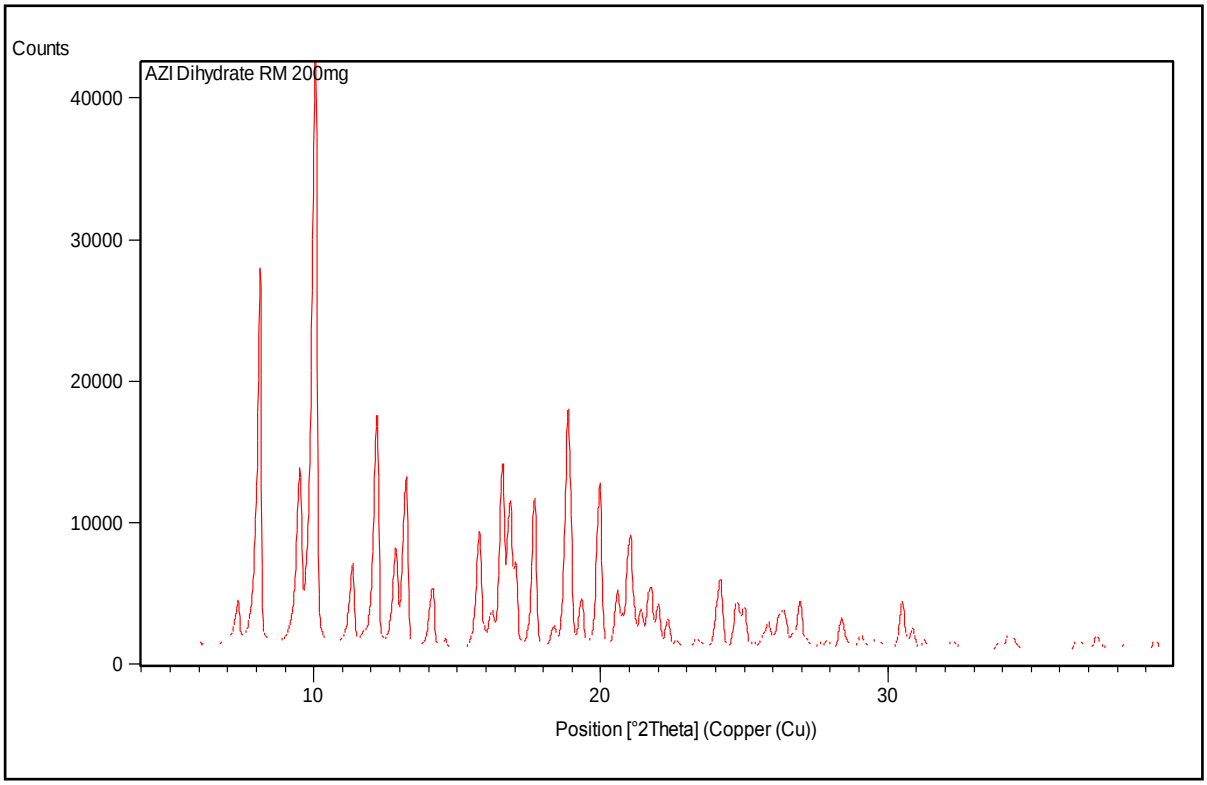

Figure 5.28 XRPD pattern for AZM-DH serving as reference during the stability study.

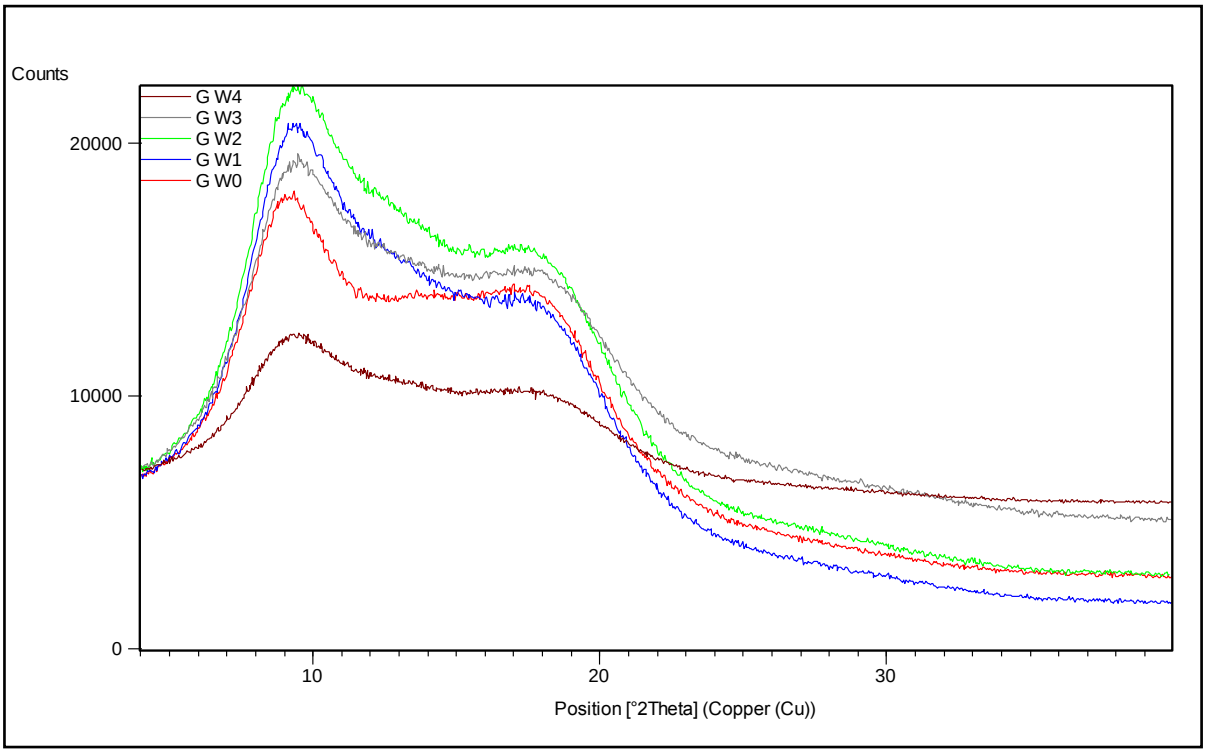

Figure 5.29 Overlay of XRPD patterns of AZM-G (unmilled) generated during the stability study (Initial (red), Week 1 (blue), Week 2 (green), Week 3 (grey), Week 4 (brown)).

5.5.2.5 Fourier transform infrared spectroscopy (FTIR)

The FTIR spectrum of AZM-DH (Figure 5.30) was generated to serve as reference for comparison of the spectra of AZM-G (unmilled), for the identification of a possible transformation from the anhydrous amorphous form into the stable AZM-DH. Figure 5.30 illustrates the characteristic peaks of AZM-DH at certain wavenumbers, compared to those of AZM-G (Figure 5.31). The relatively broad peak or multiple sharp peaks at 3500 cm^{-1} were identified as one of the main peak areas, indicative of the hydrated state of the solids, i.e. AZM-DH (the monohydrate may also form if AZM-G would start transforming, due to hydration), or AZM-G. Amorphous solids have the tendency to cause broadening of peaks on the infrared spectrum (Chieng *et al*., 2011:620; Yu *et al*., 1998:124), whereas polymorphic forms (or in this case hydrates) cause unique and characteristic peaks to shift their positions.

With reference to Figure 5.30, it is clear that AZM-DH remained stable in its crystalline, hydrated form for the duration of the stability study. No changes were visible with regards to intensity, width or absence/presence of peaks on the IR spectra of AZM-DH. As expected, as illustrated by Figure 5.31, AZM-G remained unaffected by moisture (75 % RH) during the four weeks of exposure. All of the AZM-G FTIR spectra (Figure 5.31) showed a characteristic broad peak (at 3500 cm^{-1}), whilst the rest of the spectra correlated as well. It could thus be concluded that, based on the FTIR outcomes, AZM-G remained stable at accelerated stability testing conditions over a period of at least four weeks. In comparison with the sharp peaks of the crystalline AZM-DH, the broadened peaks at 3500 cm^{-1} and 1727 cm^{-1} accentuated the amorphous nature of AZM-G (Chieng *et al*., 2011:620; Yu *et al*., 1998:124). The FTIR spectrum of AZM-G also showed many similarities to that of the anhydrous AZM reference.

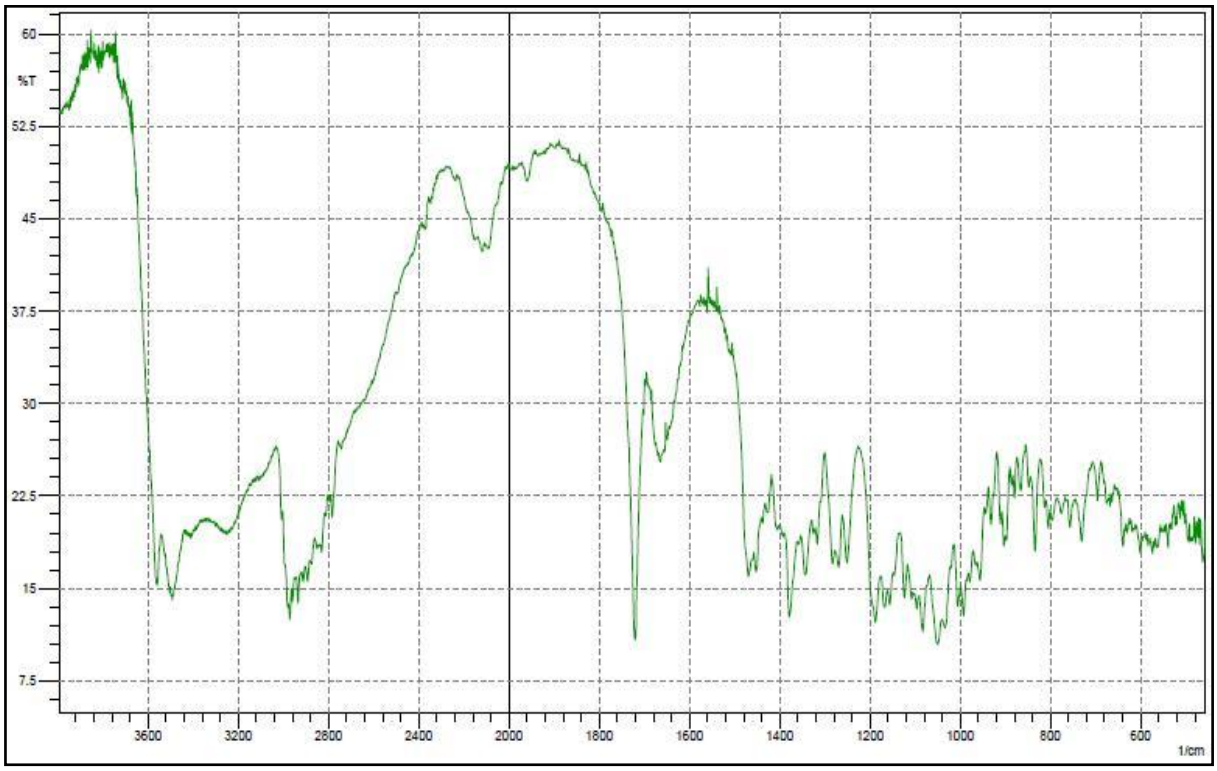

Figure 5.30 FTIR spectrum of AZM-DH that was used as the reference during the stability study.

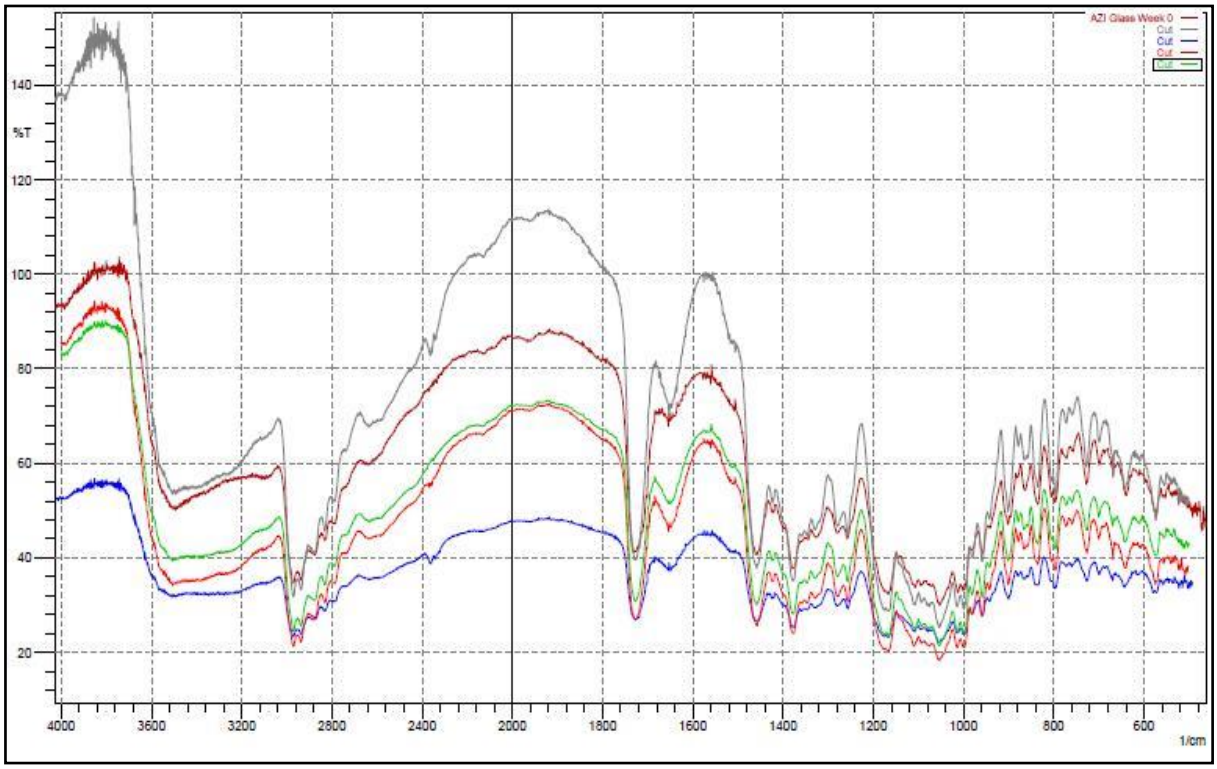

Figure 5.31 Overlay of FTIR spectra of AZM-G generated during the stability study (Initial (maroon), Week 1 (grey), Week 2 (blue), Week 3 (red), Week 4 (green)).

5.5.2.6 Microscopy

Hot stage microscopy (HSM) and scanning electron microscopy (SEM) were used for monitoring the occurrence of any possible morphological changes during the stability testing period. SEM images were taken of AZM-DH and AZM-G (unmilled). The glassy amorphous nature of AZM-G would make any morphological changes obvious under microscopic observation. The images of the initial AZM-DH sample (Figure 5.32a) were indicative of its crystalline state whilst similar crystalline structures were observed for AZM-DH (Figure 5.32b) throughout the stability study (Figure 5.33).

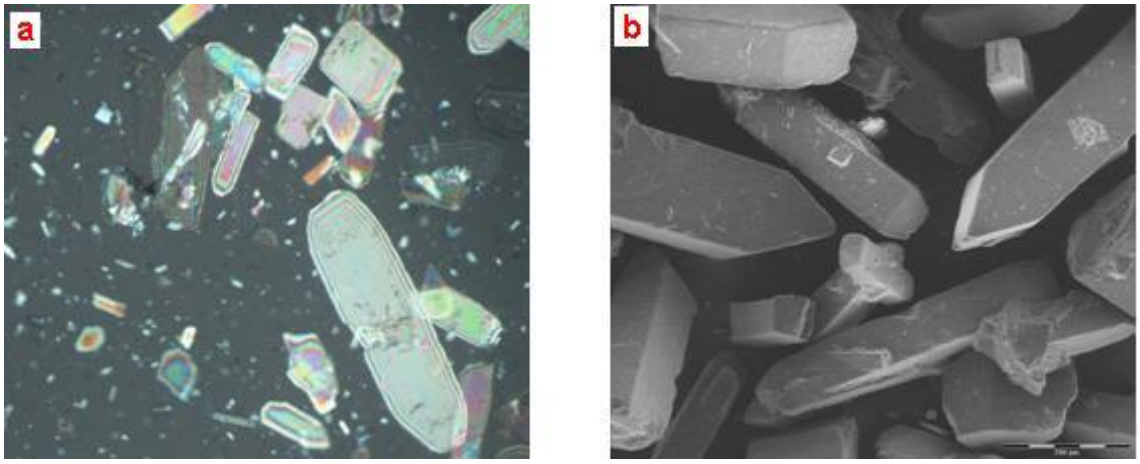

Figure 5.32 (a) HSM image of AZM-DH and (b) SEM image of AZM-DH at Week 0.

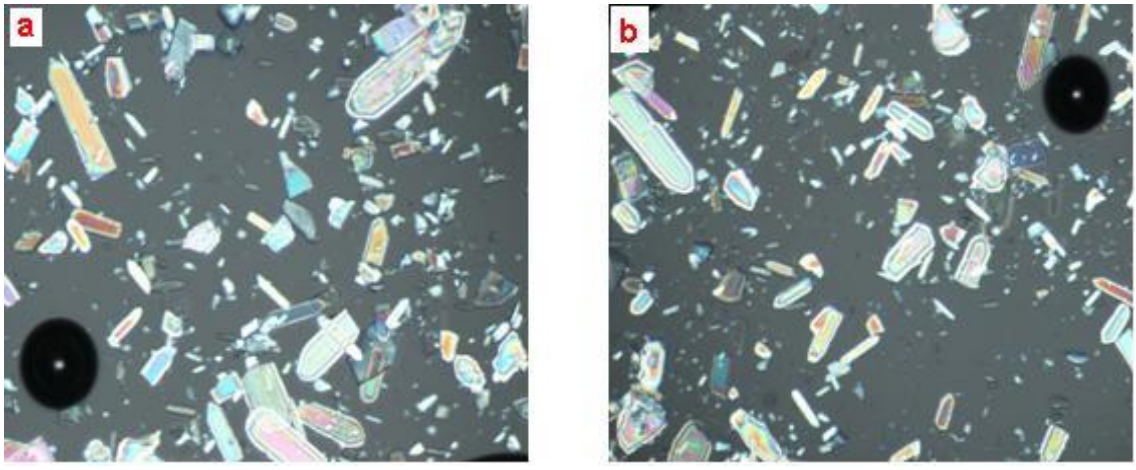

Figure 5.33 HSM images of AZM-DH at (a) Week 2 and (b) Week 4.

AZM-G (Table 5.9) images showed a very different morphology to that of AZM-DH (Figure 5.32a). The dark black spots on the images represent the silica oil that was used (as standard procedure) as sealant to cover samples to avoid/delay solvent vaporisation.

The visible glassy texture of AZM-G (unmilled) was non-crystalline, compared to the crystalline structure of AZM-DH. With reference to Table 5.9, it is clear that the non-crystalline glass retained its nature without any visible indications of transformation from the glass form into the stable, hydrated, crystalline AZM-DH. The glassy nature of AZM-G (unmilled) remained intact and could it be concluded that AZM-G was stable with regards to its morphological characteristics over the duration of the stability period.

Table 5.9 HSM images of AZM-G (unmilled) over the course of the stability study

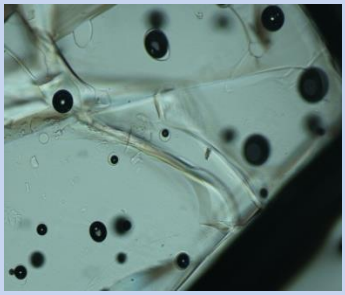	HSM image of AZM-G (Week 0).
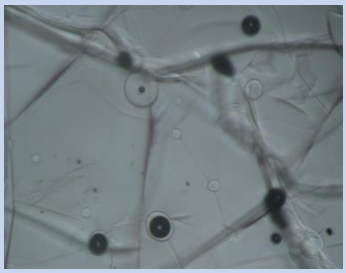	HSM image of AZM-G (Week 1).
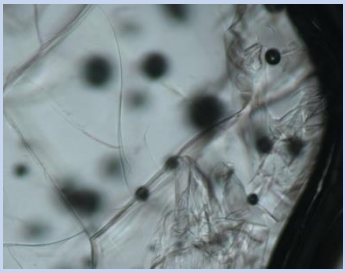	HSM image of AZM-G (Week 2).
	HSM image of AZM-G (Week 3).

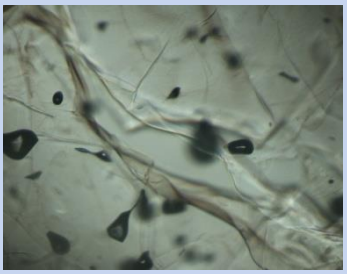

HSM image of AZM-G (Week 4).

5.5.3 Stability of AZM-G in water

As mentioned in previous paragraphs, amorphous glasses have the natural tendency of being unstable and to convert quickly into the more stable, crystalline form (Hancock & Zografi, 1997:8). The most stable form of AZM is its dihydrate. Therefore it would be expected that the anhydrous AZM-G would naturally transform into the stable, crystalline AZM-DH. This transformation should occur even more rapidly, due to the hygroscopic nature of the anhydrous AZM (Gandhi *et al*., 2002:175). However, AZM-G has proven being very stable at high humidity and temperature, as discussed in Section 5.3. Its stability was further investigated by preparing oversaturated solutions of AZM-DH, AZM-G (unmilled), and milled AZM-G in water. These solutions were left at ambient temperature in a cupboard for 20 days (no specific reason for choosing 20 days). The solutions were filtered and the filtrates dried and analysed with FTIR. This screening test resulted in the IR spectra, as illustrated by Figure 5.34.

As expected, the stable AZM-DH remained in its dihydrated form, despite being left immersed in water for a period of 20 days. Both the unmilled and milled forms of AZM-G showed signs of phase transformation into the stable, crystalline form (Figure 5.34). These spectra were similar (based on peaks at 3500 cm^{-1}) to that of AZM monohydrate, as described in the literature (Centellas *et al*., 2006:4). These FTIR spectra hence indicated a possible amorphous to monohydrate transformation (based on peaks at 3500 cm^{-1}) during 20 days of being immersed in water. These findings emphasised the true stability of AZM-G, as its transition from the amorphous state not only depended upon the presence of atmospheric water/moisture, but also upon the duration of exposure when submerged in water.

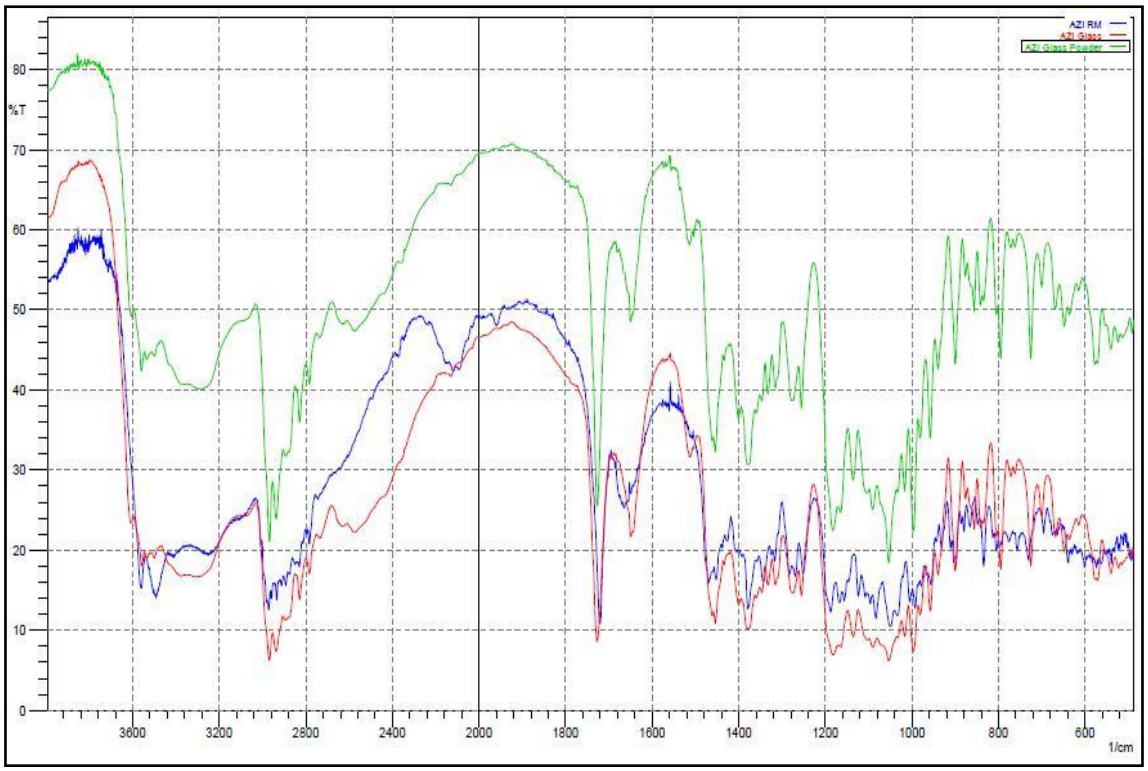

Figure 5.34 Overlay of the FTIR spectra of AZM-DH (blue), unmilled AZM-G (red) and milled AZM-G (green) after 20 days in water.

An AZM-G (milled) sample was analysed with DSC. Figure 5.35 demonstrates the result. A comparison of this thermogram of the AZM-G sample after 20 days of submersing in water, to that of normal AZM-G (Figure 5.6) and AZM-DH samples (Figure 5.5), revealed that the T_g of AZM-G had increased to 109.13˚C. The increase in T_g is referred to as the antiplasticising effect (Hancock & Zografi, 1994:471). Considering the initiation of phase transition, as illustrated by Figure 5.34, it is noteworthy that the T_g increased as a result of the onset of a change in the orientation of the molecules, which consequently shifted the T_g to the T_m of the crystalline solid. When this happens, the possibility exists that processes of melting and devitrification, or crystallisation and vitrification may occur at the same time, thus indicating that the crystal is a solid of which its T_g increased towards its T_m (Wunderlich, 2011:109). However, there were no visible signs of endotherms (representing dehydration of a monohydrate or a dihydrate), nor a melting point on the DSC thermogram (Figure 5.35). Therefore, the AZM-G had not crystallised to such an extent that the DSC thermogram analysis showed any endotherm, nor a melting point. Additional analysis was not performed at that time.

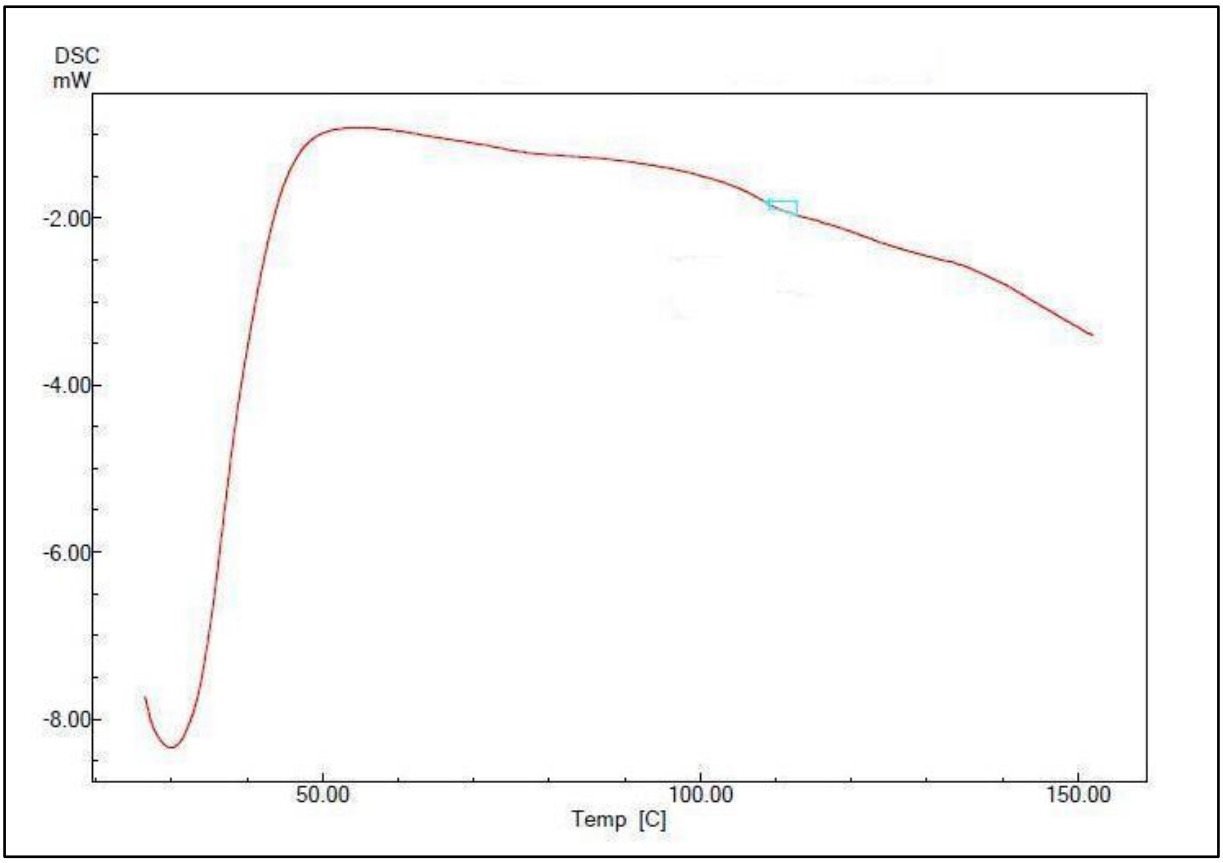

Figure 5.35 DSC trace of AZM-G (milled) indicating an endothermic event at 109.13˚C after 20 days in water.

5.5.4 Stability of AZM-G coupled with an increased water fraction

It has been mentioned that water may act as a plasticiser in glassy amorphous solids. When water is added as plasticiser, the glass transition temperature would decrease, until it reaches the point at which the molecular mobility of the solid would increase. The occurrence of more mobile molecules is due to the decrease in viscosity of the solid.

In the event that the added water has plasticised the amorphous solid to such an extent that the T_g dropped to below ambient temperature, the molecular mobility would have increased to allow the molecules to rearrange their orientations. Ultimately the rearranging molecules will accumulate uniformly as a result of nucleation and crystallisation of the solid (Aulton, 2002:145; Byrn *et al*., 1999:22; Hancock & Zografi, 1997:5; Lee *et al*., 2008:578).

Accurately weighed samples (100 mg each) of AZM-G, added to specified water fractions, were individually and thoroughly mixed using a mortar and pestle for approximately 3 minutes, where after each sample was analysed on DSC and FTIR. The water fraction

ranged from 0 - 50 %. The effect of water as plasticiser was established through the determination of the T_g of the AZM-G samples, with reference to the relevant water fraction (see Figure 5.36). The experimental mid-point T_g (K) values being generated by DSC, are given in Table 5.10. The predicted T_g (K), according to the Linear-, Gordon-Taylor- and Fox equations, are also summarised in Table 5.10.

Table 5.10 T_g values of AZM-G with increased water fraction

	Water fraction (%)								
	0	**1**	**3**	**5**	**7**	**15**	**30**	**40**	**50**
T_g of AZM-G (K)	379.80	378.71	381.95	380.48	378.84	375.90	379.43	379.63	379.95
T_g (Linear)	379.80	376.28	374.58	368.26	361.85	339.94	306.45	282.24	258.05
T_g (Gordon -Taylor)	379.80	370.93	359.12	344.32	330.79	288.34	237.10	212.40	192.98
T_g (Fox)	379.80	372.08	362.33	349.15	336.81	297.36	247.02	221.32	200.47

Referring to Table 5.10, the obvious must be stated, namely that even a 50 % water fraction had virtually no lowering effect on the T_g of AZM-G (as per the experimental T_g achieved on DSC), compared to the theoretically calculated T_g by the Linear- (Formula 5.2), Gordon-Taylor- (Formula 5.3) and Fox (Formula 5.4) equations (Figure 5.37). Figure 5.37 hence clearly illustrates that quite the opposite experimental results were obtained, than predicted. This was clearly demonstrated by the fact that the experimental curve differed substantially in terms of slope.

AZM-G thus demonstrated quite unique behaviour in the presence of water. The experimental T_g, according to the DSC, showed little or no change (decrease) in T_g with regards to the 0 % and 50 % water fractions. This implied that the water, acting as plasticiser, did not increase the molecular mobility of AZM-G and hence did not decrease the viscosity of AZM-G to allow for crystallisation to occur. For this reason, the chances of AZM-G crystallising into AZM-DH, due to water acting as a plasticiser (proven for up to a 50 % water fraction), were ruled out.

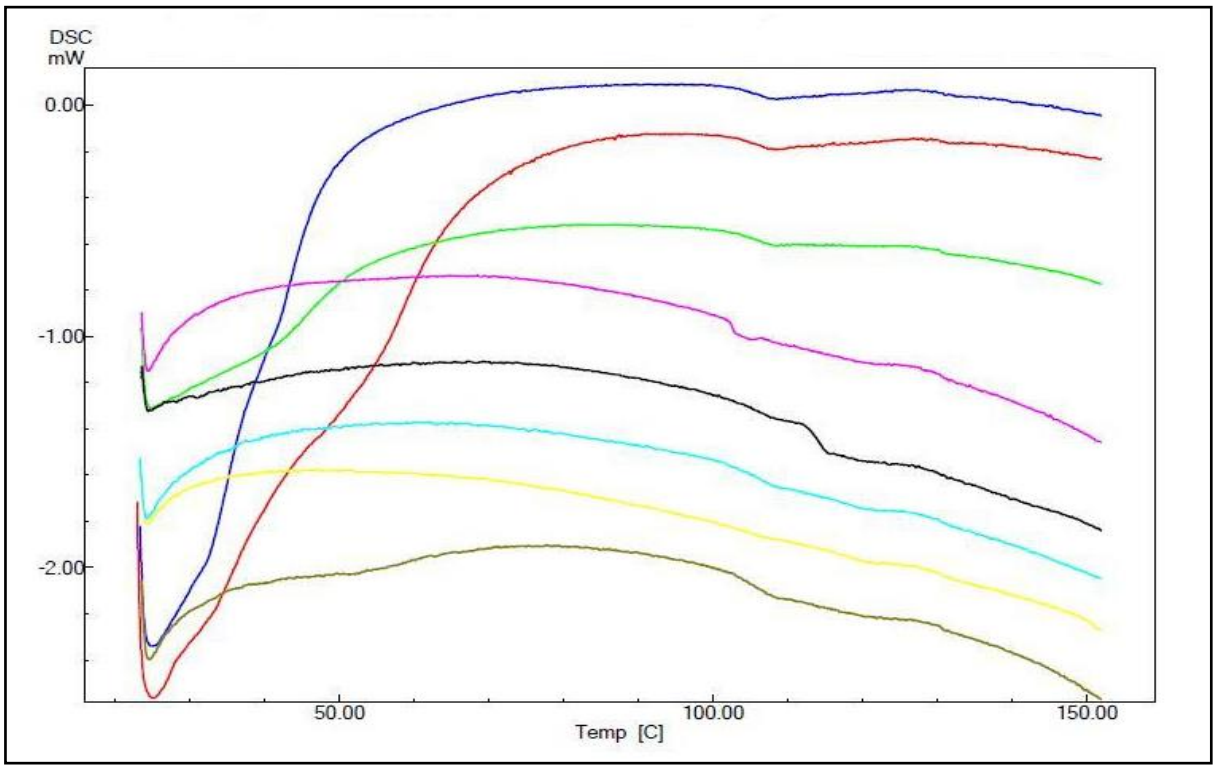

Figure 5.36 Overlay of DSC traces of AZM-G with increased water fraction, ranging from 1 - 50 %. (1 % (brown); 3 % (yellow); 5 % (light blue); 7 % (black); 15 % (magenta); 30 % (green); 40 % (red); 50 % (blue)).

The FTIR spectrum of AZM-G, having a 50 % water fraction (Figure 5.38), confirmed its stability, as it resulted in an identical FTIR spectrum to that of the initial AZM-G sample (blue). The sharp peaks in the OH-stretching region were absent, compared to the AZM-DH spectrum (black). It was hence concluded that AZM-G remained structurally stable, even in the presence of an increased water fraction. Water had no plasticising effect on AZM-G, as the T_g of AZM-G (up to a 50 % water fraction) remained similar to the initial T_g being measured (Figures 5.36 and 5.37).

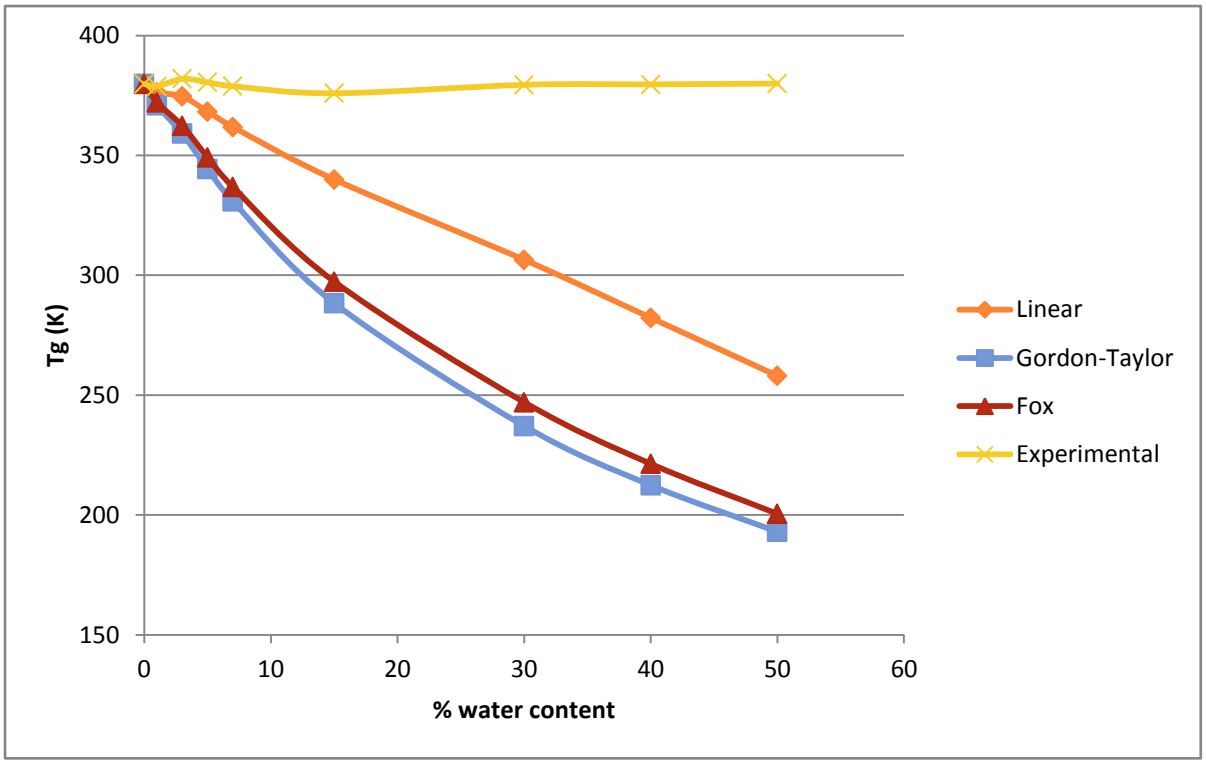

Figure 5.37 Overlay of the experimental T_g (yellow) and the T_g according to the linear- (orange), Gordon-Taylor- (blue) and the Fox equations (red).

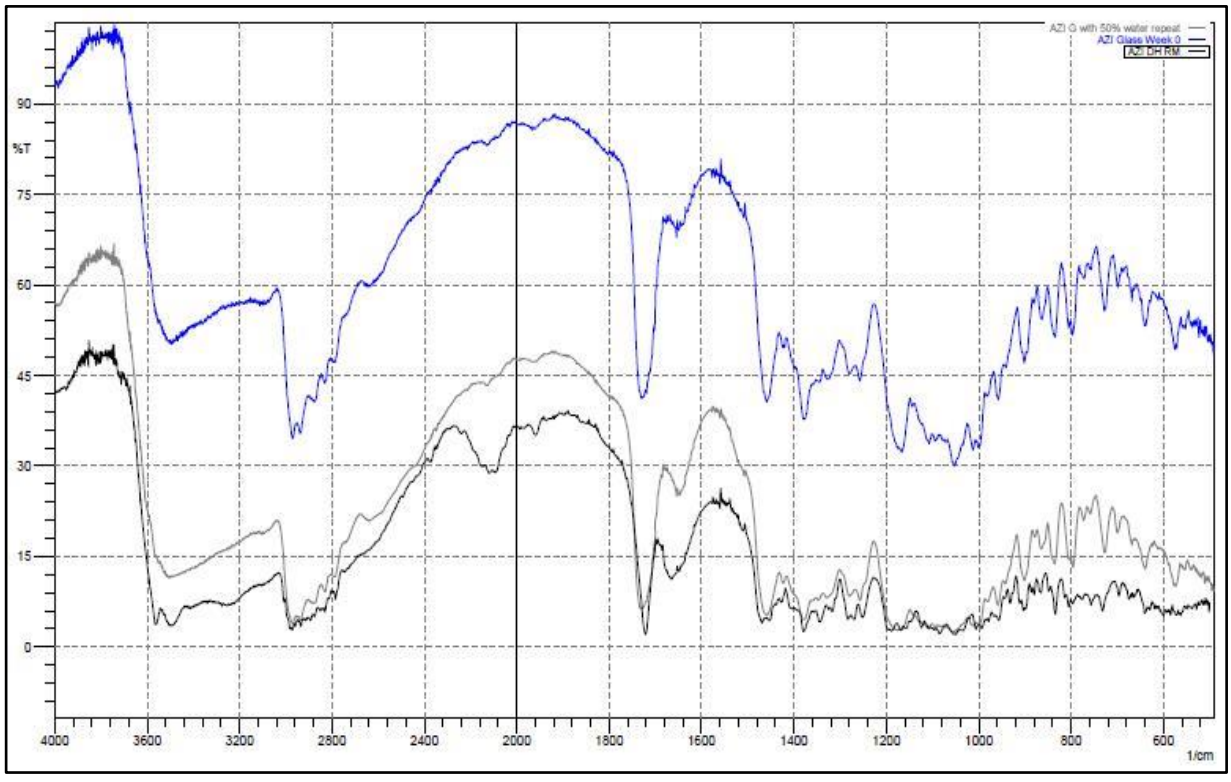

Figure 5.38 FTIR spectra of AZM-DH (black), AZM-G with 0 % water (blue), and AZM-G with an added 50 % water fraction (grey).

5.6 Conclusion

An amorphous, glassy form of AZM (AZM-G) was prepared through drying in an oven. This AZM-G was fully characterised in terms of its solid state properties. The solubility and stability of AZM-G were established, according to their respective methods, as described in Sections 2.4.3 and 2.5.1. AZM-G proved to be 339 % more soluble in water, compared to AZM-DH and was it also 39 % more soluble in phosphate buffer (pH 6.8). AZM-G furthermore remained stable at accelerated stability testing conditions of elevated temperature and relative humidity, over a period of four weeks. Exposure to very high RH (95 % and 100 %) proved to have no effect on the stability of AZM-G, as no indication of instability, nor of crystallisation existed.

AZM-G was further left immersed in water for 20 days, after which DSC results indicated that AZM-G had started to transform into the monohydrate, thus emphasising the unique stability of this glassy, solid AZM. AZM-G showed little or no interaction with water, even with exposure to a high water content of up to 50 %. The behaviour of AZM-G on exposure to water vapour and a moist environment breached almost all known models enabling the prediction of the plasticising effect of water on amorphous forms. It could thus be concluded that the stability of AZM-G was influenced by moisture, but that this interaction was exclusively time dependant, irrespective of the extent of moisture exposure.

Following the discovery during this study of its unique behaviour and stability, a solid dosage form, containing AZM-G, was envisaged. An amorphous form, exhibiting such unique characteristics, showed promising for benefiting future formulations and for improving patient compliance, because of the expectedly improved solubility rates. Overall, when considering the above characteristics, AZM-G appeared to be an example of an ideal amorphous API that could ultimately result in the improved bioavailability of azithromycin in formulation.

5.7 References

AULTON, M.E. 2002. Dissolution and solubility. (*In* Aulton, M.E., 2nded. The science of dosage form design. New York: Churchill Livingstone. p. 15-32.)

BRITISH PHARMACOPOEIA 2011. Volume V. APPENDIX A: A67, A100, A147.

BRITTAIN, H.G. 1999. Methods for the characterization of polymorphs and solvates. (*In* Brittain, H.G., Volume 95. Polymorphism in pharmaceutical solids, New York: Marcel Dekker Inc. p. 227-278.)

BRITTAIN, H.G. & FIESE, E.F. 1999. Effects of pharmaceutical processing on drug polymorphs and solvates. (*In* Brittain, H.G., Volume 95. Polymorphism in pharmaceutical solids, New York: Marcel Dekker Inc. p. 331-361.)

BYRN, S.R., PFEIFFER, R.R. & STOWELL, J.G. 1999. Solid-state chemistry of drugs. 2nd ed. Indiana: SSCI, Inc, 574 pp.

CENTALLAS, V., GARCIA, R., POCH, M., DIAGO, J., LUDESCHER, J. & BOSCH, I. 2006. Azithromycin monohydrate. Patent: EP 1 712 556 A1. 15 p.

CHAWLA, G. & BANSAL, A.K. 2009. Molecular mobility and physical stability of amorphous irbesartan. *Scientia Pharmacautica*, 77:695-709.

CHIENG, N., RADES, T. & AALTONEN, J. 2011. An overview of recent studies on the analysis of pharmaceutical polymorphs. *Journal of Pharmaceutical and Biomedical Analysis*, 55:618-644.

CRAIG, D.Q.M., ROYALL, P.G., KETT, V.L. & HOPTON, M.L. 1999. The relevance of the amorphous state to pharmaceutical dosage forms: glassy drugs and freeze dried systems. *International Journal of Pharmaceutics*, 179:179-207.

CUI, Y. 2007. A material science perspective of pharmaceutical solids. *International Journal of Pharmaceutics*, 339:3-18.

DE HARO MORENO, A., DA SILVA, M.F.C. & SALGADO, H.R.N. 2009. Stability study of azithromycin in ophthalmic preparations. *Brazilian Journal of Pharmaceutical Sciences*, 2(45):219-226.

FIESE, E.F. & STEFFEN, S.H. 1990. Comparison of the acid stability of azithromycin and erythromycin A. *Journal of Antimicrobial Chemotherapy*, 25, Suppl. A:39-47.

GANDHI, R., PILLAI, O., THILAGAVATHI, R., GOPALAKRISHNAN, B., KAUL, C.L. & PANCHAGNULA, R. 2002. Characterization of azithromycin hydrates. *European Journal of Pharmaceutical Sciences*, 16:175-184.

HAMEED, B.H., DIN, A.T.M. & AHMAD, A.L. 2006. Adsorption of methylene blue onto bamboo-based activated carbon: kinetics and equilibrium studies. *Journal of Hazardous Materials*, 141(3):819-825.

HANCOCK, B.C. & ZOGRAFI, G. 1997. Characteristics and significance of the amorphous state in pharmaceutical systems. *Journal of Pharmaceutical Sciences*, 86(1):1-12.

HANCOCK, B.C. & ZOGRAFI, G. 1994. The relationship between the glass transition temperature and the water content of amorphous pharmaceutical solids. *Pharmaceutical Research*, 4(11):471-477.

HOEPELMAN, I.M. & SCHNEIDER, M.M.E. 1995. Azithromycin: the first of the tissue-selective azalides. *International Journal of Antimicrobial Agents*, 5:145-167.

KHAN, A.R., SINGH, S.P., JAWEED MUKARRAM, S.M. & PUROHIT, M. 2002. Process for preparation of anhydrous azithromycin. Patent: EP 1 313 749 B1. 17 p.

LEE, S.L., RAW, A.S. & YU, L. 2008. Significance of drug substance physicochemical properties in regulatory quality by design. (*In* Adeyeye, M.C. & Brittain, H.G., Volume 178. Preformulation in solid dosage form development, New York: Informa Healthcare. p. 571-583.)

RAMACHANDRAN, P., VAIRAMUTHU, R. & PONNUSAMY, S. 2011. Adsorption isotherms, kinetics, thermodynamics and desorption studies of reactive orange 16 on activated carbon derived from *Ananascomosus* (L.) carbon. *ARPN Journal of Engineering and Applied Sciences*, 6(11):15-26.

RETSEMA, J. & FU, W. 2001. Macrolides: structures and microbial targets. *International Journal of Antimicrobial Agents*, 18:S3-S10.

ROUQUEROL, F., ROUQUEROL, J. & SING, K. 1999. Adsorption by powders & porous solids: principles, methodology and applications. San Diego: Academic Press, 467 pp.

THRELFALL, T.L. 1995. Analysis of organic polymorphs. *Analyst*, 120:2435-2460.

UNITED STATES PHARMACOPEIA 33, NATIONAL FORMULARY 28, REISSUE. The United States Pharmacopeial Convention, 2010 NF28 edition (2010).

VIPPAGUNTA, S.R., BRITTAIN, H.G. & GRANT, D.J.W. 2001. Crystalline solids. *Advanced Drug Delivery Reviews*, 48:3-26.

WEST, A.R. 1999. Basic solid state chemistry. 2nd ed. New York: Wiley & Sons, Ltd, 480 pp.

WU, X., LI, X. & MANSOUR, H.M. 2010. Surface analytical techniques in solid-state particle characterization for predicting performance in dry powder inhalers. *KONA Powder and Particle Journal*, 28:3-19.

WUNDERLICH, B. 2011. Phases of amorphous, crystalline, and intermediate order in microphase and nanophase systems. (*In* ŠESTÁK, J., MAREŠ, J.J. & HUBÍK, P., Volume 8. Glassy, amorphous and nano-crystalline materials: thermal physics, analysis, structure and properties, New York: Springer p. 93-114.)

YALKOWSKY, S.H. 1999. Solubility and solubilisation in aqueous media. New York: American Chemical Society, 464 p.

YU, L. 2001. Amorphous pharmaceutical solids: preparation, characterization and stabilization. *Advanced Drug Delivery Reviews*, 48:27-42.

YU, L., REUTZEL, S.M. & STEPHENSON, G.A. 1998. Physical characterization of polymorphic drugs: an integrated characterization strategy. *PSTT*, 1(3):118-127.

ZOGRAFI, G. & HANCOCK, B. 1993. Water-solid state interactions in pharmaceutical systems. (*In* CROMMELIN, D.J.A., MIDHA, K.K. & NAGAI, T. Topics in Pharmaceutical sciences, 1994, Proceedings of International Congress on Pharmaceutical Sciences F.I.P., Germany: Medpharm Scientific, p. 405-419.)